THE HEATING OF GASES BY 'DARK' DISCHARGE

by

J. E. Hesselgreaves

A thesis submitted to the Faculty of Engineering of the University of Glasgow for the degree of Doctor of Philosophy (Aeronautics and Fluid Mechanics).

SEPTEMBER 1970

ProQuest LLC.
789 East Eisenhower Parkway
P.O. Box 1346
Ann Arbor, MI 48106 – 1346

Corrigenda

p.3 Last line: insert 'a' to read: "Although a high conversion ....."

p. 5 et seq. Re-write as detailed on attached sheets

p. 9 2nd para: replace by:

"The problem of one-dimensional energy addition was also treated in a slightly different form by Nonweiler[12], and the same broad conclusions were reached."

Sec. 2.3 Under fig: "Let the temperature at the emitter be To, ..."

p.18 4th line: After eqn. 2.2 Insert "E* is the emitter field,"

p.18 4th line: $\pi/\omega - t_o$ should read $(\pi/\omega) - t_o$.

p.20 End of 2nd para last sentence should read: "..... total surface area (including the end surfaces) of an axial field heater ....."

p.23 4th line from bottom: insert "the" to read "As the applied voltage ....."

Last line: "Photos" should read "Photons"

p.24 9th line from bottom: "With further ...."

p.33 4th line: "vitrogen" should read "nitrogen"

2nd para. 2nd word: "text" should read "next"

p.34 4th line: "genxrally" should read "generally"

p.35 4th line from bottom: "prints" should read "points"

p.38 2nd para. 3rd line: insert "inversely" to read " .... inversely proportional ....

p.39 Last para: Replace 1st 8 lines by attached text.

p.44 4th para 1st line should read: "Methods of controlling heat losses have been suggested, but many more fundamental experiments on the properties of the corona discharge at high temperature and pressure would be needed before a reliable breakdown condition could be given."

4th line: erase "corona" to read " .... on the discharge ...."

p.40 Addenda: section 6.1.6 as on attached sheet.

p.61 2nd para. last sentence "suffices" should read "suffixes"

Continuation of Corrigenda

p.49 2nd line: Replace "1.3" by "1.5", "1.4" by "1.6"

4th line: Replace "1.3" by "1.5"

6th line: Replace "1.4" by "1.6"

2nd last line of text: Replace "1.17" by "1.18"

Last equation: Replace "1.17" by "1.18"

p.50 1st line: Replace "1.15, 1.16, 1.18, 1.19" by "1.16, 1.17, 1.19, 1.20"

2nd line: Replace "1.17" by "1.18"

3rd line: Replace "1.20" by "1.21"

4th line: Replace "1.12" by "1.10"

7th line: Replace "1.9" by "1.12", "1.14" by "1.15"

8th line: Replace "dV/E" by "-dV/E"

8th line: Replace "1.11" by "1.3"

9th line: Replace "1.8" by "1.12", "1.14" by "1.15"

2nd last line of text: Replace "1.13" by "1.14"

p.52 4th line: Replace "1.10, 1.2" by "1.13, 1.3"

3rd last line of text: Replace "1.10" by "1.13"

p.54 3rd and 4th lines: Erase "(c.f. equation 1.7)"

p.74 1st equation: Rewrite as "$\rho(+) = \rho_g \propto Q_o$,"

6th line: Erase "and e is the electron charge"

2nd and 3rd equations: Erase "e" in both.

Corrigenda to Notation

Add: h = specific enthalpy

Add: H = total enthalpy

Add: $\underline{j}$ = current density vector relative to neutral gas

ρ = charge density

Erase "Γ = Defined by equation 1.24" (Section re-written).

p.39 section 6.1.4: 2nd para should read as follows:

"Neither of these two uniformity requirements is likely to be closely met in practice, firstly because the energy distribution from the discharge is not uniform, being much greater near the wire, and secondly because of axial velocity gradients, both in the tube boundary layer and as a consequence of convective currents set up by the density gradients. These effects will be offset, however, by mixing caused firstly by turbulence in the tube (the Reynolds Number for the present experiments was about 2000; for the design operating condition it would be 30,000-40,000), and secondly by forced convection by virtue ...."

p.40: Addendum

6.1.6 Interaction of electric and velocity fields

It was assumed (section 2.4.1) that no interaction occurred between the electric and velocity fields. While the discharge could have a substantial effect on the gas velocity distribution (see section 6.1.4), the reverse effect should be small, since the ion velocities (of the order of 200 m/sec) are much higher than the gas velocity (1 m/sec) and its perturbations.

p.45: addendum: at bottom (Erase present last sentence)

The joint paper (ref 1), which is submitted in support of the thesis, was written by the candidate, with modifications suggested by Professor Nonweiler and Dr Foord. Sections 2.2.1 to 2.2.4 of the theory were the combined work of the candidate and Professor Nonweiler; the remainder was entirely the work of the candidate. The experiments were conducted and the results analysed by the candidate.

2. THEORY

2.1 Introduction

In the following sections the energy addition to a moving gas by gaseous ions moving in an electric field is examined. It is assumed throughout that there are no energy losses, and the effects of viscosity, and thermal and electrical conductivity are ignored; in particular the perfect gas law is assumed to apply. Direct voltage is assumed in sections 2.2 to 2.45, and 2.5, and the effects of alternating voltage are dealt with in sections 2.4.6 and 2.4.7. Steady state conditions only are treated; other assumptions are introduced where applicable.

2.2 General quasi-one dimensional theory

Consider a gas stream which is contained within an insulating duct of variable cross-sectional area A. A fraction α of the gas molecules is assumed to have a net electric charge, and a system of electrodes is arranged to give field lines which are everywhere coincident with streamlines. The basic equations describing the flow are, with the usual notation,

State $\quad p = \rho RT.$

Conservation of mass $\quad = \dot{m} = \text{constant}.$

Energy
$$\rho q \frac{dh}{dl} - q \frac{dp}{dl} = \underline{j} \cdot \underline{E} \ ,$$
where is the specific enthalpy, l is the axial length, $\underline{j}$ is the current density vector with respect to the neutral gas, and $\underline{E}$ is the electric field vector.

Momentum
$$\rho q \frac{dq}{dl} + \frac{dp}{dl} = \rho E \ ,$$
where ρ is the charge density and E is the axial component of the field vector.

Poisson's Equation
$$\nabla . \underline{E} = \frac{\rho}{\epsilon}$$
where ϵ is the gas permittivity.

Mobility Equation $\underline{V} = k\underline{E}$

where $\underline{V}$ is the drift velocity of ions with respect to the neutral gas, and k is the ion mobility.

Conservation of charge

$$\nabla . \underline{j} = 0 \quad .$$

Field strength

$$\underline{E} = -\nabla V \quad .$$

where V is the voltage.

The mass flux density ρq is given by

$$\rho q = \rho_i v_i + \rho_n v_n$$

where $\rho = \rho_i + \rho_n$ and the v's are mean velocities, subscripts i and n referring to ion and neutral gas respectively. Thus α, the ion mass fraction, is given by

$$\alpha = \rho_i / \rho \quad .$$

A parameter j is now introduced, defined by the ion mass flowrate divided by total mass flow rate. Thus

$$j = \rho_i v_i / \rho q \,,$$
$$= \alpha (1 + v/q) \,,$$

where $v = v_i - q$ = ion drift velocity with respect to the neutral gas. The equations are now put into dimensionless forms for convenience of analysis, and restriction is made to streamwise derivatives.

By taking logarithmic differentials, the equations of state and conservation of mass become, respectively :

$$\frac{dp}{p} - \frac{d\rho}{\rho} - \frac{dT}{T} = 0 \,, \qquad 1.1$$

and

$$\frac{dq}{q} + \frac{d\rho}{\rho} + \frac{dA}{A} = 0 \qquad 1.2$$

Since $E = -dV/dl$, 1.3

and, for a perfect gas,

$dh = Cp\ dT$, 1.4

the energy equation may be written

$$\frac{d(\frac{1}{2}q^2)}{CpT} + \frac{dT}{T} = -\frac{jQ_o dV}{CpT} , \quad 1.5$$

where Q_o is the charge to mass ratio of an ion.

The momentum equation becomes

$$\frac{dp}{p} + \gamma M^2 \frac{dq}{q} = -\frac{\alpha \rho Q_o dV}{p} , \quad 1.6$$

where $$M = q/(CpT(\gamma-1))^{1/2} , \quad 1.7$$

and $$\alpha \rho Q_o = \rho . \quad 1.8$$

An entropy equation may be given as

$$\frac{ds}{CpT} = \frac{dT}{T} - \frac{\gamma-1}{\gamma}\frac{dp}{p} . \quad 1.9$$

Poisson's equation becomes, by considering a tube of force

$$\frac{d(EA)}{EA} = \frac{dE}{E} + \frac{dA}{A} = -\frac{\alpha \rho Q_o dV}{\epsilon E^2} . \quad 1.10$$

The mobility equation is

$v = kE$. 1.11

It is frequently assumed (see section 6.1.2) that mobility is ~~immensely~~ inversely proportional to gas density, so equation 1.11 may be written :

$$v = k_o E . \frac{\rho_o}{\rho} \quad 1.12$$

where k_o is a constant mobility referred to a standard density ρ_o.

For conservation of charge

$$j\rho q A Q_o = i = \rho A(v + q) = \text{constant} \quad 1.13$$

where i is the total current.

For convenience of expression put

$$dW = -\frac{jQ_o dV}{CpT} = \text{specific power increment} \quad 1.14$$

and $u = \frac{v}{q} = \frac{j}{\alpha} - 1$ 1.15

The above equation ..... (continue existing text).

= = = = = = = = = = =

Replace p.8 para 2 to last para with following text.

The two possibilities to be investigated for the achievement of a substantial stagnation enthalpy gain involve operation at either high or low Mach Number. To give some impression of the limiting factors involved with high Mach Number operation, equation 1.21 is integrated for the simplified case in which the initial Mach Number is 5, the upstream (reservoir) stagnation pressure is 100 atmospheres (giving an initial density of about 1 atmosphere) and in which the product $M^2\rho$ is constant throughout the heating section.

Then since the value of the parameter $k_o^2 \rho_o/\epsilon$ is about 500 for air ions in air, the following equation is obtained:

$$(u^3 + u^2) - (u_1^3 - u_1^2) \doteq \frac{50\,(H - H_1)}{H_1}$$

where H is total enthalpy and suffix 1 denotes conditions at the beginning of the heating section.

Now the simplest breakdown condition that can be applied is that E/ρ has an upper limit; for air ions in air this means that the drift velocity v has a maximum value of about 200 m/sec. Thus with the working velocity of about 700 m/sec it is seen that u has an upper limit of 0.3, and the possible total enthalpy rise is very small; similar conclusions would be reached whatever simplifying assumptions were made.

Thus it is clear that any significant gain in enthalpy must be achieved with a large value of u, and a consequently very small Mach Number.

With the above restriction on Mach Number ..... (continue with existing text).

CONTENTS

LIST OF APPENDICES

LIST OF FIGURES

NOTATION

A = Cross sectional area or constant

B = Dimensionless variable defined by equations 2,2, 3.15, 3.18

Cp = Specific heat at constant pressure

D = $\mathrm{Exp}(B_o)$

E = Electric field strength

i = current

I = Integral defined by equation 2.7

j = ion mass flow rate/gas mass flow rate

k = Ion mobility

ℓ = axial coordinate

L = Total length of heater

$\dot{m}$ = mass flow rate of gas through heater

M = Mach Number

n = operating pressure in atmospheres

p = gas pressure

$p_r = R_1/r_o$ = cylinder ratio

P = Power

q = velocity of gas

Q_o = Charge to mass ratio of ion

r = radial coordinate

r_o = radius of central electrode

R = Radius of heater

s = specific entropy

t = T/T_o or time

T = Gas temperature

u = dimensionless parameter defined by equation 1.15

v = mean velocity of ions relative to gas

V = Voltage

dW = Specific power increment defined by equation 1.13

x = axial coordinate (section 4)

X = Dimensionless variable defined by equation 3.6

α = Ion mass fraction or 1st ionisation coefficient (section 4)

β = 2nd ionisation coefficient (section 4)

γ = Ratio specific heats or 2nd ionisation coefficient (section 4)

Γ = Defined by equation 1.24

ϵ = Gas permittivity

η = Coefficient of performance (defined by equation 3.11)

θ = Photon fraction defined fully in section 4

λ = Mean free path of gas

μ = Photon absorption coefficient of gas

ρ = Gas density

τ = Time constant (section 4)

ϕ = Constant of integration (equation 3.5)

ψ = Parameter defined preceding equation 3.5

ω = Frequency of alternating voltage

Various suffices and primes are introduced and defined where appropriate.

1. Introduction

The heating of the working gas of a hypersonic intermittent wind tunnel is normally achieved by the process of convection from a hot medium to the gas. In some cases the medium is solid (for example in a pebble bed heater); in others it is gaseous, as is effectively the case with an arc heater. All such methods suffer from the same inherent limitations of convection processes, but each has its own particular problems. A pebble bed heater, for example, is limited in run time by its finite thermal capacity, while arc heaters suffer from poor energy conversion efficiency, and are liable to problems with electrode erosion and arc control.

It is the object of this thesis to describe an investigation into the possibility of heating gases by means of a "dark" electric discharge, whereby the heating is carried out by gaseous ions liberated at one electrode and accelerated through the gas in an electric field to be neutrallised at a second electrode. Energy is thus transferred from the ions to the gas by collision; if the electrodes are suitably arranged there is also a net body force which could be used to pressurise the gas. Since heating takes place in the body of the gas a high conversion efficiency is to be expected. A stable current-voltage characteristic is expected, and electrode erosion should be negligible.

Two basic electrode geometrics are considered: an 'axial field' system, in which electric and aerodynamic flux lines ideally coincide, and body forces are taken into account; and a "radial field" arrangement, in which electric field lines are normal to the streamlines, body forces being ignored. The only ion source investigated is the corona discharge, whereby a state of partial electrical breakdown exists near the surface of a sharply curved electrode in a highly divergent field. This source was used primarily because it was the simplest, needing no ancillary equipment. Other possible sources are a spark, photoelectric emission and thermonic emission, the latter two of course yielding only negative charge carriers.

In ref.(1) a simple comparison was made between the two above geometries, and a simplified theory was given for the performance of a practical radial field heater. A fuller assessment is now made in chapter 2. In sections 2 and 3 of chapter 2 a general one-dimensional analysis is made,

from which it is concluded that low Mach-number operation is the most suitable for an axial field heater; the analysis is then extended on this assumption. Section 4 deals with the radial field heater; an equation for the temperature gradient is derived, and the numerical method of general solution is outlined. Following this an allowance is made for an alternating voltage supply; again some approximate solutions are derived and the equations are set up for numerical solutions. Finally, a comparison is made between the two heater configurations, illustrated by means of a numerical example, from which it is concluded that the radial field heater has significant advantages.

The experimental work was divided into two distinct stages, the first of which was conducted at atmospheric pressure and had the objects of

1. Verification of the theoretical current/voltage characteristics of axial and radial field heaters.

2. Determination of the efficiency of energy transfer.

The results of this series of tests were presented and discussed in Ref.(1). In summary, the theoretical assumptions were found to be largely justified, and conversion efficiency was high, although experimental errors prevented the determination of an accurate figure. On the basis of this work, and by making additional assumptions concerning the variation of breakdown field strength and ion mobility with gas density, an estimation was made of the performance of a small radial field heater to provide a gas flow of about 10 gm/sec at 500°C, working at a pressure of 15 atmospheres. The second stage of the work, described here, had the primary object of developing such a heater.

Other work related to the present investigation falls broadly into three groups:

1. A great deal of basic research on corona discharges has been carried out, principally by Loeb[2] and his co-workers, who have explained qualitatively most of the observed phenomena at pressures up to one atmosphere. Much of the earlier work was performed with point-to-plane geometries, but because field calculations are easier with cylindrical symmetry, wire-to-cylinder configurations were used for subsequent work[3].

This work was, however, chiefly concerned with identifying the various electronic mechanisms active in the discharge, and little attention was given to the factors affecting spark breakdown. In 1956 Uhlig[4] showed that the corona structure had an important effect on breakdown; his description of the form of corona required for high breakdown strength corresponds to the "steady burst pulse" state described by Loeb. Hermstein[5] suggested a method of producing this form artificially in conditions which would otherwise preclude it, thereby indicating a possible means of controlling breakdown.

2. Study of the interaction between electric and aerodynamic fields has led to two developments: the electrostatic pump and the electrogasdynamic generator. Robinson[6] performed experiments on an electrostatic blower in air at a range of pressures up to 8 atmospheres, with a point emitter and wire mesh spherical segment as collector. A series arrangement of 5 stages was also tested. A semi-empirical theory was given to describe the performance, and it was shown that gas blowers or pumps are limited to a very low electro-kinetic energy conversion efficiency. This efficiency is strongly dependent on the parameter $k^2\rho/\epsilon$, which for air ions in air is about 500, and limits the efficiency to about 1%. For insulating liquids, however, it is up to two orders of magnitude smaller, which enables efficiencies of up to 30% to be obtained[7]. Stuetzer in a more general analysis derives an upper limit of 67% based on a simple model; the potential usefulness of the energy wasted as heat was not, however, considered by either.

Electrogasdynamic power generation has been studied fairly extensively in recent years[8], and several approximate theories have been developed. Gourdine and others[9] give a thorough one-dimensional thermodynamic analysis showing the optimum relationship between energy exchanged by Joule heating and momentum change, using choking as a limiting criterion. Their analysis is incomplete, however, in that it takes no account of space charge or gas breakdown, each of which also imposes limitations on performance. Moreover experimental attention appears to have been concentrated on the use of colloidal charge carriers, the mobility of which is assumed negligible. Although high conversion

efficiency can be obtained by this means, it is evident by analogy with one-dimensional energy addition (section 2.2) that the possible power output is small.

3. Perhaps the most relevant area of related work is that of the electrostatic precipitator, since the primary object is to maximise the current for a given throughput of gas. Workers at the American Bureau of Mines[10] performed a number of experiments on models of concentric cylindrical precipitators with dust-free air at high temperature and pressure in order to obtain background information for development purposes. Air was supplied preheated to the precipitators and current/voltage measurements were made with various air temperatures up to 800^{o}C and pressures up to 5 atmospheres. Unfortunately, no measurements of the change in temperature were made, and as a consequence of the limited voltage available, breakdown data could not be obtained with positive corona. However, it was shown that stable operation of positive corona could be achieved in these conditions; negative corona became unstable at the higher temperatures. Measurements of ion mobility were made and are discussed in chapter 6.1.2.

2. Theory

2.1 Introduction

In the following sections the energy addition to a moving gas by gaseous ions moving in an electric field is examined. It is assumed throughout that there are no energy losses, and the effects of viscosity, and thermal and electrical conductivity are ignored; the perfect gas law is assumed to apply. Direct voltage is assumed until sections 2.2 to 2.4.5 and 2.5, and the effects of alternating voltage are specifically dealt with (section 2.4.6); other assumptions are introduced where applicable.

2.2 General quasi-one dimensional theory

Consider a gas stream which is contained within an insulating duct of variable cross-sectional area A. A fraction α of the gas molecules is assumed to have a net electric charge, and a system of electrodes is arranged to give field lines which are everywhere coincident with streamlines. The equations describing the flow in steady state are, with the usual notation:

State $$\frac{dp}{p} - \frac{d\rho}{\rho} - \frac{dT}{T} = 0 \qquad 1.1$$

Conservation of mass $$\frac{dq}{q} + \frac{d\rho}{\rho} + \frac{dA}{A} = 0 \qquad 1.2$$

where q is the velocity of the gas.

Energy $$\frac{d\left(\frac{1}{2}q^2\right)}{C_p T} + \frac{dT}{T} = -\frac{j Q_o dV}{C_p T} \qquad 1.3$$

where j = ion mass flow rate/gas mass flow rate,

Q_o = charge to mass ratio of ion.

Thus jQ_o = specific current

(Note that dV will take a negative sign when Q_o is positive).

Momentum $$\frac{dp}{p} + \gamma M^2 \frac{dq}{q} = -\frac{\alpha \rho Q_o dV}{p} \qquad 1.4$$

where α = ion mass fraction ,

$$M = q/(C_p T(\gamma - 1))^{1/2} \qquad 1.5$$

= local Mach number of gas

Entropy $$\frac{ds}{C_p T} = \frac{dT}{T} - \frac{\gamma - 1}{\gamma} \frac{dp}{p} \qquad 1.6$$

Poisson's equation

$$\frac{d(EA)}{d\ell} = \frac{\alpha \rho Q_o A}{\epsilon} \qquad 1.7$$

where E = electric field strength

ϵ = permittivity of gas

ℓ = axial distance along duct.

The electrical quantities are also liked by the following relationships:

Mobility equation $$v = kE \qquad 1.8$$

where v = mean velocity of ions relative to bulk gas velocity

and k = ion mobility.

It is normally assumed (see section 6.1.2) that mobility is inversely proportional to gas density, so equation (1.8) may be written

$$v = k_o E \frac{\rho_o}{\rho} \qquad 1.9$$

where k_o is a constant mobility "normalised" to a standard density ρ_o.

Conservation of charge

$$j \rho q A Q_o = i \qquad 1.10$$

where i = current,

and $\rho q A$ = $\dot{m}$ = mass flow rate 1.10a

It follows directly from the definitions of j, α and ν that j and α can be linked by the equation

$$\alpha(\nu+q) = j\,q. \qquad 1.11$$

Finally, $$E = -dV/dl \qquad 1.12$$

By the use of equation (1.12), l may be eliminated and Poisson's equation may be put into a dimensionless form:

$$\frac{d(EA)}{EA} = \frac{dE}{E} + \frac{dA}{A} = -\frac{\alpha\rho Q_o\,dV}{\epsilon E^2} \qquad 1.13$$

For convenience of expression put

$$dW = -\frac{j Q_o\,dV}{C_p T} = \text{specific power increment}, \qquad 1.14$$

and $$u = \frac{\nu}{q} = \frac{j}{\alpha} - 1 . \qquad 1.15$$

The above equations form a set of simultaneous equations which can now be solved for the reduced derivatives dp/p etc. The area change dA/A and energy addition term dW are chosen as control variables, after the method of Shapiro and Hawthorne[11], and the Mach number M, and u, are used as parameters. Solutions for dT/T and du/u are given in Appendix I, and the results are summarised below.

$$\frac{dp}{p} = -dW.\frac{\gamma M^2}{1-M^2}\left[1 - \frac{1}{u+1}\left(1 + \frac{1}{(\gamma-1)M^2}\right)\right] + \frac{dA}{A}.\frac{\gamma M^2}{1-M^2} \qquad 1.16$$

$$\frac{d\rho}{\rho} = -dW.\frac{1}{1-M^2}\left[1 - \frac{\gamma}{\gamma-1}.\frac{1}{u+1}\right] + \frac{dA}{A}.\frac{M^2}{1-M^2} \qquad 1.17$$

$$\frac{dT}{T} = dW.\frac{1}{1-M^2}\left[1 - \gamma M^2.\frac{u}{u+1}\right] + \frac{dA}{A}\,\frac{(\gamma-1)M^2}{1-M^2} \qquad 1.18$$

$$\frac{dM^2}{M^2} = dW.\frac{1}{1-M^2}\left[1 + \gamma M^2\left\{1 - \frac{1}{u+1}\left(\frac{2}{(\gamma-1)M^2}+1\right)\right\}\right] - \frac{dA}{A}.\frac{2\left(1 - \frac{\gamma-1}{2}M^2\right)}{1-M^2} \qquad 1.19$$

$$\frac{ds}{C_p T} = dW.\frac{u}{u+1} \qquad 1.20$$

$$\frac{du}{u} = dW.\frac{k_o^2\rho_o}{\epsilon}.\frac{\rho_o}{\rho}.\frac{1}{u^3+u^2}.\frac{1}{M^2(\gamma-1)} \qquad 1.21$$

These equations are now in a form suitable for numerical integration, once "starting" values of M, u and ρ_o/ρ have been specified, and increments of power addition (dW) and area change (dA/A) decided. In order to establish these starting values it is necessary to consider the requirements of the heater, which are that a large enthalpy rise of the gas must be achieved in the minimum volume of duct, without a significant pressure drop, without such an area change that the one-dimensional treatment is invalidated, and within the restrictions imposed by the condition of electrical breakdown of the gas.

The relationship between the parameters M and u, which control the pressure change, is dictated by equation 1.21, the modified form of Poisson's equation. Now from equations 1.9, 1.10a and 1.15, it is easily shown that (see Appendix I)

$$\frac{du}{u} = \frac{dE}{E} + \frac{dA}{A} \qquad 1.22$$

so that equation 1.21 relates the change in field strength to the energy addition. The simplest spark breakdown condition that can be applied to the gas is that the quantity E/ρ has an upper limit; this requires that $dE/E - d\rho/\rho$ be small (say of order dW at maximum). Expanded with the aid of equation 1.21, this becomes, after re-arrangement

$$\frac{dE}{E} - \frac{d\rho}{\rho} = dW\left(\Gamma + \frac{1}{1-M^2}\left(1 - \frac{\gamma}{\gamma-1}\cdot\frac{1}{u+1}\right)\right) - \frac{dA}{A}\cdot\frac{1}{1-M^2}, \qquad 1.23$$

where $$\Gamma = \frac{k_o^2 \rho_o}{\epsilon}\cdot\frac{\rho_o}{\rho}\cdot\frac{1}{u^3+u^2}\cdot\frac{1}{M^2(\gamma-1)} \qquad 1.24$$

For a given duct, the value of the term $\frac{1}{1-M^2}\left(1 - \frac{\gamma}{\gamma-1}\cdot\frac{1}{u+1}\right)$ is at maximum of order unity, so the multiplying factor of dW in equation 1.23 depends entirely on the value of Γ. Since the value of the parameter $k_o^2\rho_o/\epsilon$ is about 500 for air ions in air, inspection of 1.24 reveals that the product $M^2 u^3 \rho/\rho_o$ must be very much greater than unity, or, for practical values of working pressure, $M^2 u^3 \gg 1$. But equation 1.16 shows that to avoid considerable pressure loss, $M \ll 1$, so that $u \ggg 1$.

With the above restriction on Mach Number it is clear from equations 1.16 to 1.18 that the effect of area change on the properties of state is small; thus there appears to be little loss in generality in

confining consideration to constant area flow with its associated simplicity of analysis. This case is treated more fully in the following section.

The above is necessarily an incomplete discussion on one-dimensional energy addition; the subject was also treated in a slightly different form by Nonweiler[12], and the same broad conclusions were reached.

2.3 Axial field heating at low Mach Number

Consider now the flow in a constant area duct with $M \ll 1$, and $u \ggg 1$. Thus $\frac{dp}{p} \ll dW$, and $dT/T \doteq -d\rho/\rho \doteq dW$

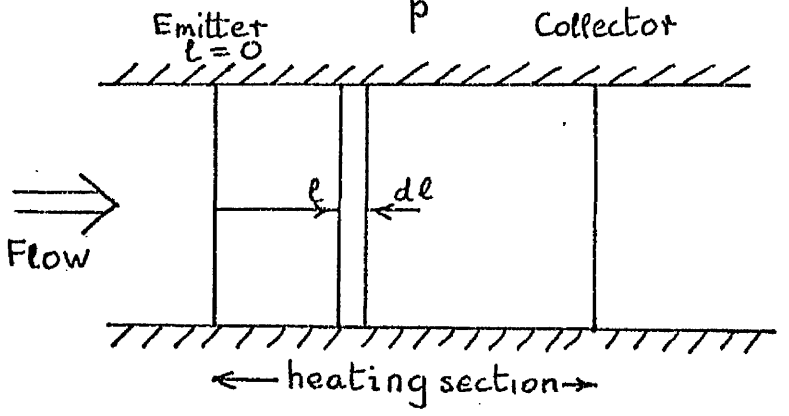

Let the temperature at the emitter T_o, be the same as ambient, and the pressure-constant throughout — be n atmospheres.

With the above simplifications equations 1.18 and 1.21 may be combined to give

$$\frac{dT}{T} = \frac{E^2 dE . \epsilon A k_o}{n \dot{m} C_p T_o} \qquad 2.1$$

which could be more easily obtained by working from simplified forms of the basic equations 1.3, 1.7, 1.9, 1.10 and 1.12.

For optimum operation the maximum field strength E_c at the collector must correspond to the breakdown strength. Then integration of 2.1 yields (see Appendix II):

$$\left(\frac{T_c}{T_o}\right)^3 \ln\left(\frac{T_c}{T_o}\right) = B_f . n^3 \left(1 - \left(\frac{E^*}{E_c}\right)^3\right) \qquad 2.2$$

where $$B_f = \frac{\epsilon A k_o E_{\beta,a}}{3 \dot{m} C_p T_o n} , \qquad 2.3$$

and $E_{b,a}$ is the breakdown field strength at atmospheric conditions, for an axial or one-dimensional field. Equation 2.2 thus provides a relationship between mass flow rate, cross-sectional area and operating pressure, for operation near gas breakdown.

The length L of the heating section is obtained by consideration of equations 1.12 and 1.18 together with 1.10 and 1.14:

$$L = \frac{V}{n E_{b,a}} \cdot \frac{1}{1 - T_o/T_c} \int_1^{T_c/T_o} \left(\frac{\ln\left(\frac{T_c D}{T_o}\right)}{\ln\left(\frac{T D}{T_o}\right)} \right)^{1/3} d\left(T/T_o\right) \qquad 2.4$$

where V = applied voltage,

$D = \exp(B_o)$,

and $B_o = \frac{\epsilon A k_o E^{*3}}{3 \dot{m} C_p T_o n}$

The derivation of equation 2.4 is given in Appendix II.

2.4 Theory of the radial field heater

2.4.1 Introduction

A radial field is produced by the maintenance of a potential difference between concentric cylinders; the inner cylinder can conveniently be a wire, and if the potential difference is great enough the stress at the surface of the wire is sufficient for corona formation, where upon a radial current flows. A radial field heater thus consists of such an arrangement with an axial flow of gas which becomes heated by the discharge. It is evident that the gas velocity field lines are not coincident with electric field lines; there is assumed to be no interaction between the two fields. In general, the outer cylinder radius is allowed to vary along its axis, with the limitation that the axial component of the field strength and its derivatives are small.

The basic assumptions made in the theory additional to those mentioned in section 2.1 are that

a) The electrodes are ideally smooth and concentric

b) Ionisation in the gas is confined to a small region immediately surrounding the wire. The thickness of this region is ignored.

c) Ion mobility is dependent only on gas properties.

d) Gas pressure is constant throughout the heater.

e) Gas temperature is independent of radius.

f) The perfect gas law is applicable.

The current-voltage relationship of this geometry is first discussed and then used to predict the heater performance.

2.4.2 Current-voltage relationship (direct voltage)

A number of investigators have studied the relationship between current and applied voltage for an arrangement of concentric cylinders, using various assumptions concerning the boundary condition at the inner cylinder (hereafter referred to as the wire). The general form of the relationship is always an implicit expression for the current in terms of the voltage, however, and most investigators make small-current approximations in order to obtain a simplified explicit relationship. The method developed here appears to have been first derived by Townsend[13].

Consider a cross-section of cylindrical duct, as shown below, of internal radius R_1 and with a concentric wire of radius r_o. A potential difference V_a is maintained between these electrodes; the problem is to find the current i in terms of V_a, R_1 and r_o for given conditions of the intervening gas, and to express it in a form suitable for the heater theory.

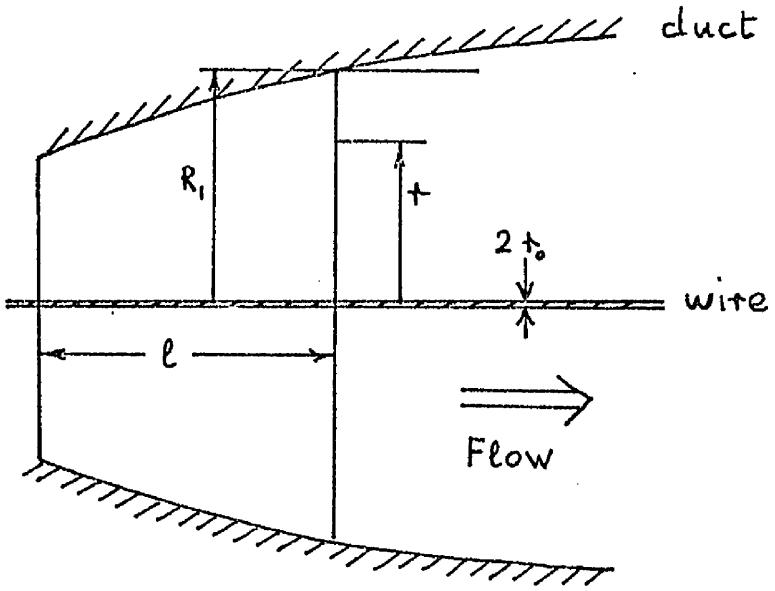

Townsend's solution, which is derived in Appendix III, is of the form:

$$\frac{V_2 X}{\psi^{1/2} r_0} = (1+X^2 p_r^2)^{1/2} - (1+X^2)^{1/2} + \ln p_r + \ln\left(\frac{1+(1+X^2)^{1/2}}{1+(1+X^2 p_r^2)^{1/2}}\right), \quad 3.1$$

where $X^2 = \dfrac{\psi}{E_r^{*2} - \psi}$, [dimensionless] 3.2

$$\psi = \frac{di/dl}{2\pi\epsilon k}, \quad 3.3$$

$$p_r = R_1/r_0, \quad 3.4$$

E_r^* is the starting field strength at the wire, and k is the local mobility.

The relationship may also be written

$$\frac{di}{dl} = 2\pi\epsilon k \eta \left(\frac{V_2}{R_1 - r_0}\right)^2, \quad 3.5$$

where $$\eta = X^2(p_r - 1)^2 \Big/ \left[(1+X^2 p_r^2)^{1/2} - (1+X^2)^{1/2} + \ln p_r + \ln\left(\frac{1+(1+X^2)^{1/2}}{1+(1+X^2 p_r^2)^{1/2}}\right)\right]. \quad 3.6$$

The value of η depends only upon X and p_r; it is zero when the current is zero and approaches its maximum value of unity as either p_r or X tends to infinity. The latter occurs as $\psi \to E_r^{*2}$, so that there is a theoretical upper limit to the current (and hence voltage). The parameter η may thus be regarded as a convenient coefficient of performance. In practice spark breakdown usually occurs before the upper limit is reached. The physical significance of the limit follows from equation III.viii (Appendix III); as $X \to \infty$ the field strength becomes uniform and equal to the starting field strength, at which it has been assumed that local "breakdown" occurs.

If the current is very small the current-voltage relationship is linear (see Appendix III), while at higher currents equation 3.5 shows that it tends to a quadratic function as η approaches unity.

It is convenient, especially for section 2.4.6, to know how η varies with applied voltage, and in order to non-dimensionalise the relationship, a "starting voltage", V_0, is defined as that at which corona is just formed. From equations 3.1 and 3.2, as $\psi \to 0$, the well-known result is obtained:

$$V_o = E_t^* r_o \ln p_t \qquad 3.7$$

Combination of equation 3.7 with 3.5 and 3.3. then gives

$$\frac{V_2}{V_o} = \frac{X(p_t - 1)}{(1+X^2)^{1/2} \eta^{1/2} \ln p_t} \qquad 3.8$$

By the use of X as a parameter, η may be calculated from 3.6 and substituted into 3.8 to obtain V_2/V_o. Fig. (1) shows η plotted against V_2/V_o for various values of p_r.

2.4.3 The heating equations

Consider the elemental volume of cylindrical duct shown below.

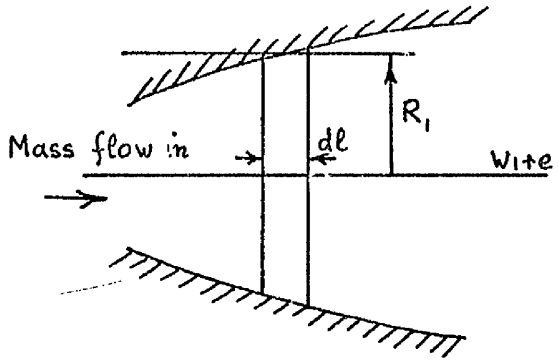

Let the cylinder radius be $R = R(\ell)$. Then the increment of power input to the volume is, from equation 3.1.5,

$$V_2 \, di = \frac{2\pi \epsilon k \eta V_2^3 \, d\ell}{(R_1 - r_o)^2} \qquad 3.9$$

From assumptions (d) and (e), and equations 1.10, 1.14 and 1.18, the energy equation is

$$\frac{dT}{T} = \frac{V_2 \, di}{\dot{m} C_p T} \qquad 3.10$$

Equations 3.9 and 3.10 may now be combined to give

$$\frac{dT}{T} = \frac{2\pi \epsilon k \eta V_2^3 \, d\ell}{\dot{m} C_p (R_1 - r_o)^2 T} \qquad 3.11$$

This equation gives the temperature gradient along the duct in terms of the applied voltage and mass flow rate, and is used as the basis for all the subsequent heating analysis. It cannot easily be integrated directly, since η is an implicit function of V_2, and of k, which is temperature dependent. Two simplified solutions may be obtained, however, by the assumptions that η = unity and that ion mobility and breakdown field strength are directly proportional to density (see sections 6.1.2 and 6.3); these solutions are given in ref.(1) for a typical heater specification, and represent the ideal maxima obtainable with constant-radius and variable-radius heaters. The curves are shown on fig.(2), and the shape of the optimum heater is shown on fig.(3).

The methods of the complete solutions are now given; the Algol procedures used for the numerical computations are given in Appendix V.

2.4.4 General solution: constant radius case

Consider now the real situation in which p_r and X are finite, so that η is less than unity. In order to set up equation 3.11 for numerical integration the following steps are involved:

1. The mobility k is expressed as

$$k = k_o . k\left(n, T_\ell/T_o\right), \qquad 3.12$$

where k_o is the mobility at standard (atmospheric) conditions, and $k\left(n, T_\ell/T_o\right)$ is a dimensionless function of operating pressure, represented by n, and local temperature (T_ℓ/T_o).

2. Since the applied voltage is constant, the radius R_1 is determined by the breakdown condition at the downstream end. It is assumed (see section 6.3) that the ratio V_2/R_1 at breakdown is dependent only on gas pressure and temperature; this relationship is written as

$$\left(\frac{V_2}{R_1}\right)_{B_+} = E_{\ell,+} . E_m\left(n, T_\ell/T_o\right) \qquad 3.13$$

where $E_{\ell,+}$ corresponds to $(V_2/R_1)_{\text{Breakdown}}$ at atmospheric conditions (see Ref.1), and E_m is a dimensionless function of pressure and temperature. A similar expression is also used for the starting field (see Appendix VI).

Thus if the required exit temperature is given by T_f/T_o, equation 3.13 gives

$$R_1 = \frac{V_2}{E_{b,r} \cdot E_m(n, T_f/T_o)} \qquad 3.14$$

3. The value of η is found at each step of the integration by the formation of the variable X of equation 3.6; this is an iterative process and is described in Appendix IV.

By the incorporation of the above steps, the heating equation 3.11 may be written in finite difference form as

$$\frac{\Delta T}{T_o} = B_1 \cdot E_m(n, T_f/T_o) \cdot k(n, T_\ell/T_o) \cdot \frac{\eta}{(1-1/p_r)^2} \cdot \frac{\Delta \ell}{R_1} , \qquad 3.15$$

where $B_1 = \frac{2\pi \epsilon k_o V_2^2 E_{b,r}}{\dot{m} C_p T_o}$. (Compare with B_ℓ of section 2.3)

The constants k_o, $E_{b,r}$, V_2, $\dot{m}$ and C_p are assumed to be known from experiment or requirement, and the functions E_m and k by experiment. A suitable interval $\Delta \ell / R_1$ is chosen. The equation is then integrated step by step, the temperature calculated at each stage being used in the functions k and E_m. The process is repeated until the desired exit temperature T_f is reached (at which point breakdown is assumed to occur). The length of heater is obtained during the course of integration by counting the increments $\Delta \ell / R_1$.

Fig. 2 shows the temperature distribution thus calculated, for a range of values of the parameter $\tau \left(= \frac{E_{o,r}}{E_{b,r}} \right.$: see Appendix IV$\left.\right)$, to the following heater specification:

$E_{b,r}$ = 10 kV/cm; V_2 = 100 kV; $\dot{m}$ = 10 gm/sec; n = 15 atmospheres; T_o = 293°K; p_r = 100; T_f/T_o = 3.0 (not attained within scale of graph).

It is seen that the curves all have a form similar to that of the corresponding simplified solution (ref.1), which is exponential. For convenience it was assumed that corona field and breakdown field were each proportional to density, and that mobility was inversely proportional to density.

2.4.5 General solution: variable radius case

The intention here, as in the simplified case considered in ref.(1), is to maintain a near-breakdown condition over the whole length of tube, and similar assumptions are used. Assume that the wire radius r_o is fixed, so that p_r is variable, and that $(V_2/R_1)_{Br}$, E_r^* and k are dependent on gas pressure and temperature, as before.

Thus $$\left(\frac{V_2}{R_1(\ell)}\right)_{Breakdown} = E_{\ell,\tau} \cdot E_m(n, T\ell/T_o) \cdot \qquad 3.16$$

Now define the heater inlet radius as R_s, so that

$$R_s = \frac{V_2}{E_{\ell,\tau} \cdot E_m(n,1)} \cdot \qquad 3.17$$

Substitution of these relationships into equation 3.11 as before gives

$$\frac{\Delta T}{T_o} = B_2 \cdot E_m^2(n, T\ell/T_o) \cdot k(n, T\ell/T_o) \cdot E_m(n,1) \cdot \frac{\eta}{(1-1/p_\tau)^2} \cdot \frac{\Delta \ell}{R_s} \qquad 3.18$$

where $$B_2 = \frac{2\pi\epsilon k_o R_s^2 E_{\ell,\tau}^3}{\dot{m} C_p T_o}$$

The calculation of η follows the form given above for the constant radius case, modified by the fact that p_r is variable; this is given by

$$p_\tau = \frac{R_1(\ell)}{r_o} = \frac{V_2}{r_o E_{\ell,\tau} E_m(n, T\ell/T_o)} \quad \text{(from equation 3.16)}$$

i.e. $$p_\tau = p_{\tau s} \cdot \frac{E_m(n,1)}{E_m(n, T\ell/T_o)}, \qquad 3.19$$

where p_{rs} is the cylinder ratio at entry to the heater.

Equation 3.18 may now be integrated as before, by starting from the known gas conditions at inlet.

The shape of the heater is given by

$$R_1(\ell) = r_o \cdot p_\tau$$

$$= \frac{R_s}{p_{\tau s}} \cdot p_\tau \qquad 3.20$$

Fig.(2) shows the temperatures distributions obtained for a performance the same as that of the constant radius heater, with a starting cylinder ratio of 30. The curves approach closely to the ideal of ref.(1). The corresponding shapes of the heaters are shown in fig.(3).

2.4.6 Modification for alternating voltage supply

Suppose the supply voltage is sinusoidal with an angular frequency ω. We now examine the effect of this on the performance of the heater. It is assumed that the instantaneous current at any instantaneous voltage is the same as the current at that direct voltage, implying that the capacitance of the electrode system must be negligibly small. An approximate criterion for this is derived in Appendix VII.

By examination of equation 3.16 of the direct voltage analysis, it is seen that η may be regarded as an index of effectiveness of power input, being the ratio between the actual power input and the theoretical limit of input (for the same applied voltage). This ratio is now called $\eta_{d.c}$, and an "a.c. effectiveness", $\eta_{a.c}$ is defined as the ratio between the mean power absorbed from an alternating supply and the same (d.c.) limit, the peak voltage corresponding to the d.c. value. The problem now is to find $\eta_{a.c}$ in terms of the applied voltage, in a similar form to that presented on fig.(1) for $\eta_{d.c}$. The method of solution adopted is to integrate the instantaneous power over a quarter cycle, it being assumed that the current waveforms for the two polarities are identical. The situation may be described by means of the diagram.

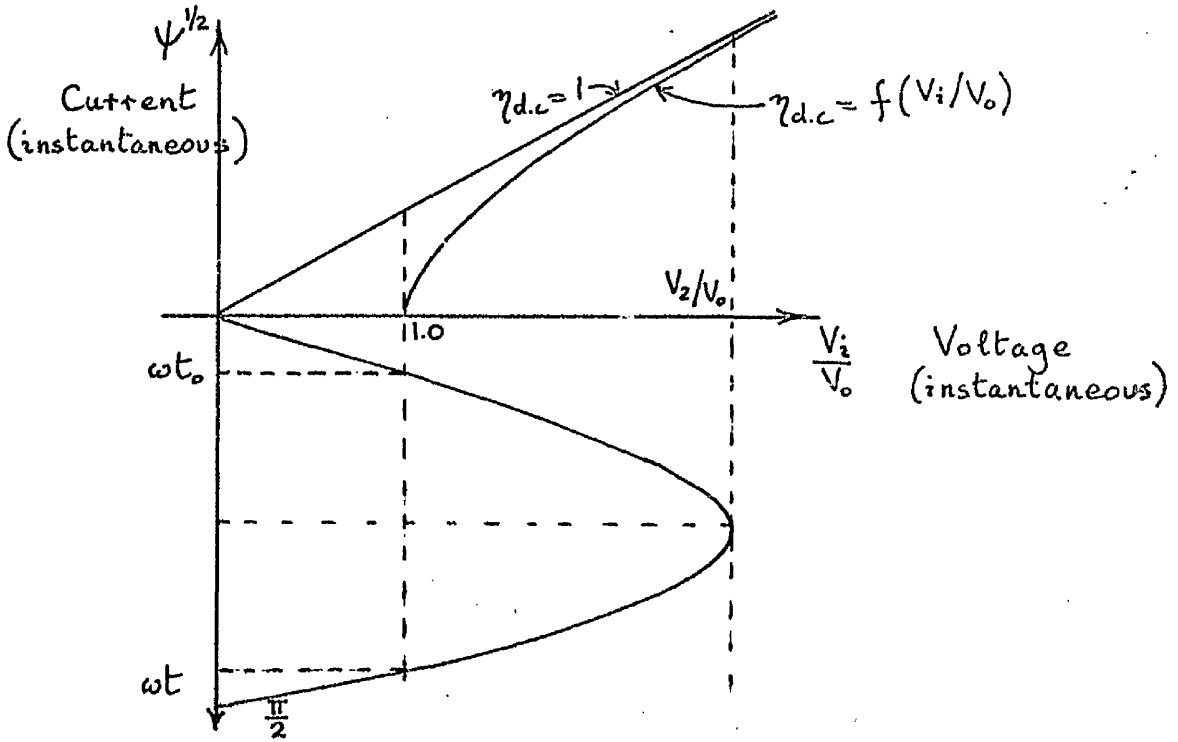

The instantaneous voltage is given, by definition, as

$$\frac{V_i}{V_o} = \frac{V_2}{V_o} \sin\omega t \qquad 4.1$$

The instantaneous current, represented by ψ (see equation 3.3), is zero up to the time t_o and after a time $\pi/\omega - t_o$, where $t_o = \frac{1}{\omega} \arcsin V_o/V_2$. Between these limits it follows the relationship given by equation 3.5:

$$\psi_i = \frac{\eta_{d.c}\, V_i^2}{(1-1/p_r)^2 R_i^2}, \qquad 4.2$$

where the subscript i refers to the instantaneous value.

The details of calculation are described in Appendix VIII, and yield the result:

$$\eta_{a.c} = \frac{2}{\pi}\int_0^{X_2} \frac{X^4}{(1+X^2)^2}\left(\frac{V_o}{V_2}\right)^4 \frac{(p_r-1)^3}{\eta_{d.c}^{1/2}(\ln p_r)^4}\left(1-\frac{1}{(1+X^2)\eta_{d.c}}\left(\frac{V_o}{V_2}\right)^2\frac{p_r^2}{(\ln p_r)^2}\right)^{1/2}\{A(X)\}\,dX, \qquad 4.3$$

where $$A(X) = \left\{\frac{p_r^2}{1+(1+X^2p_r^2)^{1/2}} - \frac{1}{1+(1+X^2)^{1/2}} - \frac{X(p_r-1)}{(1+X^2)\eta_{d.c}^{1/2}}\right\},$$

$$\left(\frac{V_o}{V_2}\right)^2 = \frac{(\ln p_r)^2(1+X_2^2)(\eta_{dc})_{X_2}}{p_r^2 X_2^2 (1+1/p_r)^2},$$

X is the instantaneous value of X corresponding to ψ_i, and X_2 is the value of X at the peak voltage V_2.

The function is shown plotted versus V_2/V_o on figure (4), and is asymptotic to a value $4/3\pi$ as $V_2/V_o \to \infty$. Three simplified solutions also given in Appendix VIII have the same limiting value. The Algol procedure used for integration of equation 4.3 is given in Appendix IX.

2.4.7 The effect of alternating voltage supply on heater performance

Since $\eta_{a.c}$ is found in terms of the same parameters, X and p_+ as $\eta_{d.c}$, a simple substitution of $\eta_{a.c}$ for η in the equations 3.26 (section 2.4.3) and 3.32 (section 2.3.4) will give the a.c. heater performance. The parameters X_2 and $(\eta_{dc})_{X_2}$ have of course to be evaluated first from the applied (peak) voltage, using the method described in Appendix IV.

2.5 Comparison between axial and radial field heaters

The principal factors to be considered in the choice of a heater for a given duty are those of overall shape and the complexity of the electrode system. These are now dealt with in turn.

From Appendix II.2 the shape of an axial field heater of circular cross-section may be represented by

$$\left(\frac{L^2}{R^2}\right)_{axial} = \frac{\pi . \epsilon k_o V_2^2 E_{b,a}}{3 \dot{m} C_p T_o} \cdot \frac{I^2}{(1-1/t_c)^2 t_c^3 \ln(Dt_c)} , \qquad \text{II.ix}$$

where $$I = \int_1^{t_c} \left(\frac{\ln(Dt_c)}{\ln(Dt)}\right)^{1/3} dt ,$$

and $t = T/T_o$, t_c referring to the collector.

For a radial field heater, the assumption that ion mobility is proportional to density gives, by integration of equation 3.11 for a constant radius R_1:

$$\frac{T}{T_o} = \exp\left(\frac{2\pi\epsilon k_o}{\dot{m} C_p T_o} \cdot \frac{L}{R_1} \cdot V_2^2 \eta E_{b,r} \cdot \frac{T_o}{T}\right), \qquad \text{II.x}$$

where η is an overall heater effectiveness.

Thus $$\left(\frac{L}{R_1}\right)_{radial} = \frac{\dot{m} C_p T_o t_c \ln t_c}{2\eta\pi\epsilon k_o V_2^2 E_{b,r}} . \qquad \text{II.xi}$$

Division of equation II.ix by II.xi gives

$$\frac{(L^2/R^2)_{axial}}{(L/R)_{radial}} = \frac{E_{b,a}}{E_{b,r}} \cdot \frac{2\eta}{3} \cdot \frac{I^2}{t_c^4 (1-1/t_c)^2 \ln t_c \ln(Dt_c)} \qquad \text{II.xii}$$

Substitution of a typical set of design values ($t_c = 2.7$, $V_a = 100$ kV, $\dot{m} = 10$ gm/sec, $k_o = 2$ cm^2/volt.sec., $E_{b,a} = E_{b,r} = 10$ kV/cm) for a small heater reveals that

$$\left(\frac{L}{R}\right)_{axial} \ll 1 \text{ , and } \left(\frac{L}{R}\right)_{radial} \gg 1 .$$

Now for heat losses to be a minimum, the shape factors would each have to be around unity to obtain a small surface area. In each case this requirement could only be met if the applied voltage were very high. Voltages above 100 kV, however, would raise considerable practical difficulties owing to insulation requirements, so it must be concluded that the above shape factors are unavoidable, and since for the purposes of expanding the heated gas through a nozzle the flow must be constricted to a very small diameter, the radial heater would seem preferable. To illustrate this point the above example is expanded, since it corresponds to the pilot model envisaged in ref.(1) and investigated in this report. It has already been seen that at 15 atmospheres pressure the radial field heater has a diameter of about 3 cm and a length of about 1 metre; substitution of the requisite numbers into equation 2.4 for an axial field heater yields a length of 2 cm and a diameter of about 0.75 metre. It is evident that the total surface area of an axial field heater would be much the greater, with consequently greater heat losses.

The other main factor to be considered in the comparison is that of the electrodes. For each heater the electrode system would have to satisfy the assumed electrical boundary conditions as closely as possible, and for the axial heater the electrodes would also have to be permeable to the gas. Considering the latter gas, a wire mesh screen would be suitable for the collector, provided that the melting point of the metal used was well above the operating temperature. The emitter (c.f. ref.1) would typically be an arrangement of fine points in uniform distribution across the emitter plane. Such an arrangement for a large diameter would be of considerable complexity, especially when it is borne in mind that the points need frequent replacement when run at high current densities. The

staging of several such heaters in series in order to reduce the diameter would be possible but wasteful of space, since neutrallisation zones at least equal to the gap length would be necessary. Insulation problems would also be severe.

A radial field electrode system would suffer from none of these disadvantages, and it is concluded on both theoretical and practical grounds that this geometry is preferable.

3. The Corona Discharge

3.1 Introduction

The concept of heating by dark discharge considered in the work described here is based on the corona discharge, whereby a very small region of ionised gas provides a source of charge carriers which pervade the rest of the inter-electrode volume. It is assumed that the power required for ionisation is small compared with the total power delivered (see section 6.1.3).

Although the corona region plays no direct part in the analysis - indeed its dimensions are assumed negligible - it is useful to gain an understanding of the mechanisms involved in the discharge, since they control the spark breakdown condition, which sets the upper limit to heater performance. Most of the research on corona processes has been performed with point-to-plane geometries (Ref.2,p.938 et seq.) in connection with studies on secondary ionisation phenomena, but there is no fundamental difference between point-to-plane and wire-to-cylinder corona. There are, however, differences between positive and negative polarity, and these are now treated separately. Breakdown is more fully discussed in chapter 4 and section 6.3.

3.2 Negative corona

When the point, or wire, is acting as the cathode, the discharge consists of a series of regular pulses of electrons (Ref. 2, p 938 et seq.), which follow very narrow discharge channels, or streamers, outwards from the cathode. The electrons are emitted by a variety of processes, including positive ion bombardment, field emission and photoelectric emission. Initially the electrons are drawn by the high field; they are then rapidly accelerated to high energy, and create positive ion/electron pairs by collision with neutral molecules. The positive ions then bombard the cathode, creating more electrons. The "pulse" thus formed is eventually choked by the formation of a space charge of negative ions further out in the field, which reduces the field strength at the cathode. A new pulse is formed when the negative ions have drifted

clear towards the anode. As the applied voltage is increased the pulses become longer in duration until eventually the resultant current to the anode is a steady direct value with a high frequency ripple superimposed. Another consequence of the increasing voltage is that electrons remain at high velocity further from the cathode; this delays their attachment to oxygen atoms and molecules, with the result that the effective mobility of the ions is increased[10]. Ultimately, with further increase in voltage, a pulse crosses the gap before it can dissipate, and the low resistance channel thus formed leads to a spark.

The above tendency for the carriers to remain as electrons leads to an inherent instability, particularly at high temperatures[10], as the stabilising influence depends on the reduction of cathode field by the negative ion space charge. Negative corona is thus thought to be fundamentally unsuitable for the purposes of dark discharge heating.

3.3 Positive corona

Positive corona is also basically a pulsed phenomenon, having three fairly distinct phases of operation with a common fundamental mechanism, which is the first phase described below.

Phase I

The fundamental mechanism is initiated by electrons liberated by random processes in the gas, such as thermal ionisation and cosmic rays. The electrons which are not immediately attached to neutral particles move in rapidly towards the anode, and when they have gained sufficient energy they ionise the gas. The resultant electrons cause further ionisation before being neutralised at the anode, while the positive ions drift outwards at a much lower velocity. Since high fields exist only very close to the anode, the electrons only exist in large quantities in this region, while the positive ions traverse almost the whole gap. The positive space charge near the anode reduces the local field strength, preventing further ionisation until it has drifted away, thereby causing the pulsing effect[13]. As applied voltage is raised the pulses become larger and form "streamer" channels. These carry sufficient positive charge for them to attract electrons, which cause further ionisation and excitation of neutral particles. Photos from the latter process also aid

in promoting further ionisation in the neighbourhood of the streamer tip. Growth of the streamer is stopped when the local field strength is not sufficient to promote ionisation; spark breakdown occurs when a sufficiently large pulse of ions reaches the cathode at high energy, to release a return stroke of electrons.

Phase II

The second phase of corona consists of streamers formed in the same way, but Hermstein[5] has shown that a small negative ion space charge is present near the anode under some conditions which has a controlling influence on the streamers and greatly alters both the outward appearance of the discharge and the breakdown condition. Its formation is rather complicated, being connected with the process of decay of streamers, but the main requirement is that the field strength near the anode must be very high and highly divergent. Thus with reference to a concentric cylindrical electrode system, if the cylinder ratio p_r is high (say greater than 200 at atmospheric conditions), streamers will form initially on application of a voltage greater than the starting voltage (defined in section 2.4.2). These will usually be visible as a violet diffuse glow and will be audible as an irregular hissing. As the applied voltage is raised, sufficient numbers of negative ions are produced which escape recombination and arrive to form a close sheath around the anode. Their effect is to enhance the field at the anode surface but to reduce the field outside the sheath; the latter effect serves to prevent growth of streamers beyond the sheath boundary. This phase corresponds to the "steady burst pulse corona" described by Loeb (Ref.2 p.952). It is inaudible, and the glow is much fainter and closer to the anode surface than that of the streamer phase I. The charge pulses are much smaller and more uniform than those of phase I. In further increase of voltage a further slight reduction in size is noticed, but eventually because of the increase in current, the field outside the sheath can rise to the value necessary for streamer propagation. Since the field becomes also much more uniform with high current (see equation III.viii) spark breakdown may occur very suddenly. Hermstein[5] showed, however, that an external control can be imposed by the introduction of negative ions from an external source; this was shown to extend the range of voltage within which suppression of streamers takes place.

Phase III

The remaining phase of operation occurs when the cylinder ratio is very high (e.g. greater than 400 at atmospheric conditions); the discharge then takes the form of discrete tufts regularly spaced along the wire. Each tuft appears to be composed of a large number of streamers similar to those of phase I. The tufts increase in number as voltage is raised, but no explanation of their formation appears to have been given. It may be that this form is analogous to that of the point-to-plane geometry, for which there is known to be a constricting mechanism[14]. Sparking from this phase is erratic, but is generally at a low voltage compared with that of phase II. Further reference to these phases is made in the discussion in section 6.3.

4. Spark Breakdown

In this chapter the basic mechanisms of the spark discharge in relation to the axial field and radial field geometrics are outlined in turn. Practical aspects are considered in chapter 7.

4.1 Breakdown in a uniform field

Sparking between parallel or quasi-parallel electrodes has been one of the most widely studied of gaseous breakdown processes, and has led to the common but misleading references to the "breakdown field strength" of a gas. It would in fact be very difficult to measure such a field strength, since the presence of electrodes is a necessary prerequisite for such studies, and breakdown streamers, although able to propagate purely by gaseous processes, are invariably initiated at electrode surfaces. Thus in referring to the breakdown of a gas it is strictly speaking necessary to allow for the shape, material, and surface condition of the electrodes.

Townsend was the first to obtain a condition for gaseous breakdown; by defining the coefficients α and β to be the number of ion pairs produced per unit distance of travel through the gas by the collision with neutral molecules of electrons and positive ions respectively, he showed (Ref.2, p.751 et seq.) that an artificially produced current at the cathode became infinite in a uniform field when

$$\alpha = \beta \exp(\alpha - \beta)x \qquad 4.1$$

where x is the distance between the electrodes. Thus if α and β are known as a function of the field strength the sparking voltage can be calculated. However, it was soon shown that β was far too small, in the majority of situations, to have any direct effect on breakdown, and β was replaced as a secondary process by γ_i (Ref.2, loc cit), the number of electrons liberated at the cathode by the impact of a positive ion. The breakdown condition then becomes

$$1 = \gamma_i(\exp(\alpha x) - 1) \qquad 4.2$$

From this equation, and using the semi-empirical relationship

$$\frac{\alpha}{p} = A \exp\left(-\frac{Bp}{E}\right) \qquad 4.3$$

given by Townsend, where A and B are constants for the gas, it is easily shown that

$$V_s = \frac{B.px}{\ln\left(\frac{A.px}{\ln(1/\gamma_i)}\right)}, \qquad 4.4$$

where V_s is the sparking voltage. Equation 4.4. would perhaps be better expressed more generally as

$$\frac{V_s}{V_I} = \frac{B'(x/\lambda)}{\ln\left(\frac{A'x/\lambda}{\ln(1/\gamma_i)}\right)} \qquad 4.5$$

where V_I is, say, the first ionisation potential of the gas, λ is the mean free path, and A' and B' are revised dimensionless coefficients. Thus within the range of applicability of equations 4.2 and 4.3, the sparking voltage is a function of the product of gas density and gap length; this is the well known similarity rule for spark gaps. In general, however, it is likely that several secondary mechanisms are in operation simultaneously, and also that space charges play an appreciable part in the process. If positive ion action and photoelectric action are taken in account, but the effect of local space charges is ignored, it has been shown by Loeb (Ref. 2, p.861) that the breakdown condition becomes

$$1 = \frac{\alpha\gamma_i}{\alpha - 1/\tau v}\left\{\exp\left(\alpha - 1/\tau v_+\right)x - 1\right\} + \frac{gf\theta}{\alpha - \mu - 1/\tau v}\left\{\exp\left(\alpha - \mu - 1/\tau v_-\right)x - 1\right\} \qquad 4.6$$

where $1/v$ represents the sum $1/v_+ + 1/v_-$, v_+ and v_- being the draft velocities of the carriers, τ is a time constant related to the growth rate of space charge in the propagating streamer, g is a geometrical factor related to photon arrival at the cathode, θ is the fraction of photons to liberate electrons which escape back-diffusion, μ is the photon absorption coefficient of the gas, $f(x')$ is the photon-production ratio at x' per electron produced, and

Equation 4.6 contains statistical factors[15] and is clearly of such complexity that a simple expression such as equation 4.5 for a breakdown voltage or field would be impossible to derive. In fact the concept of a well-defined breakdown voltage loses its meaning when the above mechanisms are present; a more realistic viewpoint would be to consider the probability of a spark at a given voltage within a given time of application of that voltage. This concept has given rise to much recent work on time lag studies (Ref. 2, p.751,864).

4.2 Breakdown in a non-uniform field

When the field strength is not uniform across the gap the breakdown condition is given by the integral relationship (of which equation 4.6 is a simplification):

$$1 = \gamma_i \int_0^x \alpha \left[\exp\left(\int_0^{x'} \left(\alpha - \frac{1}{v\tau} \right) dx' \right) \right] dx' + g\theta \int_0^x f(x') \exp\left(\int_0^{x'} \left(\alpha - \frac{1}{v\tau} \right) dx' - \mu x' \right) dx' \qquad 4.7$$

Clearly although the field (for a concentric cylindrical configuration) could be calculated from equation III.viii (Appendix III), the problem is more intractable than the uniform field case. It must also be borne in mind that factors such as electrode material and surface texture, and gas temperature and composition may play an important part in the breakdown process, neither of which are allowed for in the above.

It thus seems unlikely that a reliable theoretical breakdown condition can be derived at present; the only alleviating factors are that the field strength for a concentric cylindrical arrangement tends towards uniformity as voltage is increased (see section 2.4.2), and that experiment may reveal that certain ionisation mechanisms are predominant in the region of interest thus simplifying calculations. Alternatively it may be possible to exercise a form of external control to achieve a similar effect, as suggested in section 3.3.

5. Experiments

5.1 Introduction

The first stage of the experimental work was conducted at atmospheric pressure (Ref.1), and, as stated in the main introduction, had the objects of verification of the current-voltage characteristics of the two geometries, and determination of the efficiency of energy transfer. A perspex cylinder of about 11 cm diameter and 40 cm in length was used as the test duct, and various combinations of emitter and collector geometrics were tested. Both axial field and radial field results agreed well with theory, in spite of the inevitable lack of correspondence of electrical and aerodynamic boundary conditions. In all configurations the efficiency of energy transfer was high, and the results as a whole were sufficiently encouraging to warrant further experiments at high pressure.

The primary aim of the second stage, described here, was to develop a radial-field heater designed, with the aid of a breakdown assumption, on the theory of ref.(1). A constant radius heater was to be tested first to establish the validity of the theory and the breakdown assumption; the information gained was then to be used in the design of an optimum heater.

5.2 General arrangement of apparatus

An overall view of the apparatus is given in fig(5); more detail is shown in fig.(6) and a schematic diagram of the gas supply is shown in fig.(7). The heater, shown also in fig.(8), was mounted in a large pressure vessel which was supplied with gas from high pressure cylinders through a gland in the bottom end plate (fig.(9)). On passing through the heater the gas was passed to atmosphere through a control valve. Electrical power at high voltage (up to 80 kV) was supplied via a rectifier system (section 5.4.2) to a bushing on the top end plate of the vessel (fig. 5).

5.3 Pressure vessel

The pressure vessel consisted of two sections bolted end to end, each being two feet in length and one foot square. Box section stiffeners were welded circumferentially at two positions along each section (fig. (5)), and flanges were welded on to take circular endplates. One endplate was adapted to take the high voltage bushing, the other being adapted for the heater mounting internally and gas connections externally (see figs.(9) and (8)). "O" ring seals were inserted between the sections, at the endplate and the above fittings. A pneumatic relief valve acted as a safeguard, and also allowed for rapid exhaustion of the vessel. A gland in the vessel wall was adapted for electrical connections to be made between the heater and external measuring equipment.

The vessel was mounted on a large steel frame with provision for vertical movement to allow for accommodation of a vacuum chamber beneath; this facility was designed for the intended development of a low density wind tunnel. Because of the considerable weight of the lower endplate, a wire suspension was arranged whereby it could be manoeuvred by means of a chain pulley system (fig.(8)).

Before use with gas the vessel was hydraulically tested up to 250 p.s.i. gauge. For this purpose transformer oil was used as the test fluid, since water, and possibly hydraulic fluid, would have damaged the insulation of the high voltage bushing. The pressure was taken up to 250 p.s.i. several times, and in one case was left for several hours without sign of leakage.

5.4 Measurement systems

5.4.1 Gas supply and measurement

High pressure cylinders were arranged (fig.7) to operate either singly or in parallel to supply gas to the vessel via a regulator valve and control panel. A Platon flowmeter calibrated by the manufacturers was used in series with a fine control valve to monitor the gas flow to the pressure vessel. A line in parallel with the flowmeter provided for rapid filling of the vessel prior to tests. The input line pressure, which at low flow rates is equal to vessel pressure, was measured downstream of these

fittings by a Budenburg six-inch diameter Bourdon-type gauge. The control panel also contained the outlet valve to the chamber, so that pressure and flow rate could be controlled simultaneously.

Measurement of gas flow rate through the heater was made by adding an increment to the input value calculated from the rate of pressure change in the vessel during the tests (see section 5.6.1).

5.4.2 Electrical supply and measurement

Power at direct voltage was supplied from mains by a 10 kVA, 50 kV transformer in conjunction with a solenium plate rectifier unit, which operated in a Cockcroft-Walton doubler arrangement to give 100 kV at 100 mA. A 0.06 μF capacitor was used for smoothing; the ripple factor was found to be less than 5% at no load, and up to 10% under working loads. The applied voltage was measured by monitoring the current passing through a 400 mΩ resistor bank across the load, the system having an estimated accuracy of about 4%. An Avometer was used to measure the current across the heater. The circuit was as given in ref.(1).

5.4.3 Gas temperature measurement

In the light of previous experience with platinum resistance thermometers[1] it was thought desirable to position the thermocouple for outlet gas temperature measurement so as to obtain the maximum possible electrical shielding. The thermocouple was accordingly inserted and bonded into the brass connection on the vessel endplate, the hot junction being placed on the centreline. An ice bucket was used to provide a fixed cold junction temperature. The location is shown on fig.(9).

The heater inlet temperature was assumed to be equal to the ambient (laboratory) temperature.

5.5 Description of heater

The development of the heater is described in Appendix X. The arrangement consisted essentially of a stainless steel tube of 2.8 cm internal diameter, fitted with 6 mm thick, 10 cm diameter flanges at each end (fig. 8). A length of 79 cm was chosen, being the maximum that could be accommodated in the pressure vessel after space allowances for insulators and the H.T. bushing had been made.

In order that electrical measurements could be made the heater tube was insulated from the vessel endplate by ceramic insulators. The arrangement is shown on fig.(8) with the endplate ready for raising and attachment. The insulators illustrated are to the original design, which proved unsatisfactory (see Appendix X); the final versions are shown on figs.(12) and (13). Tufnol bolts held the assemblies together, and at the lower end P.T.F.E. gaskets were inserted to prevent leakage of gas into the heater. The emitter wire was located (see Appendix X) by spiders mounted in the insulators, and was held in tension by a coil spring attachment at the upper end. A P.T.F.E. spider was inserted along the wire to prevent excess vibration (fig. 11). A similar attachment made electrical contact with the electrode of the high tension bushing in the pressure vessel.

5.6 Heater performance tests

The experimental programme had two main objects, to be pursued concurrently:

1. To find the efficiency of energy conversion of the heater at stages of increasing mass flow rate and pressure up to design values of each, for the constant radius heater.

2. To check the validity of the theoretical assumptions, especially the variation of ion mobility and spark breakdown voltage with density and temperature, in order to facilitate development of a variable-radius heater.

5.6.1 Energy conversion; results and discussion

A measurement of electrical to thermal energy transfer efficiency was made by comparing the enthalpy output with electrical power input, the former being obtained by measuring the output gas temperature and flow rate, and the latter from current and applied voltage measurements. The temperature measured at the centre-line of the duct at outlet was assumed to be the mean temperature of the gas; any refinement obtained by assumption of a temperature profile was thought unjustifiable at this stage.

In order to avoid wastage of gas while both the electrode system and experimental procedure were under development, the vessel pressure was not taken above 80 p.s.i.g. for these tests. The gas used was oxygen-free vitrogen, which was supplied in 625 ft^3 cylinders at 2000 p.s.i.g. No effort was made to exhaust the vessel before filling, so that the gas passing through the heater was a variable mixture of atmospheric air and nitrogen. It was not thought that this had any significant effect upon the measurements, as the thermodynamic properties of air and nitrogen are similar, and a difference in ionisation phenomena is only encountered when pure nitrogen is used.

The text procedure was firstly to fill the vessel to the desired pressure by means of the flowmeter bypass valve, and to set up a given influx of gas using the fine control valve (fig.7) in series with the flowmeter. The vessel outlet valve was then opened and adjusted so that the pressure remained as nearly constant as possible, thus equalising the input and output flow rates. Any deviation was accounted for by timing the pressure change over the period of the run and making a small correction. The applied voltage was then raised until the desired power level was reached, whereupon a pause was necessary to allow the system to gain its "equilibrium" temperature. This was assumed to have occurred when no further increase in output gas temperature was measureable, an average time being about 20 minutes. Temperature measurement was made difficult by large fluctuations of the galvonometer needle, which were probably caused by turbulence in the gas at the probe, since they were still present when power was switched off, but disappeared when the flow was shut off.

Results of measurements of conversion efficiency are shown in figs 14 and 15, for a variety of input powers up to the spark breakdown point, and for several flow rates. A table of results is also presented in Table I.

The maximum performance achieved at an operating pressure of about 3 atmospheres was a temperature rise of $68^{\circ}C$ with a mass flow rate of 1.25 gm/sec and a conversion efficiency of 0.37, while at 5.4 atmospheres a maximum temperature rise of $87^{\circ}C$ was obtained, with the same mass flow rate and an efficiency of 0.453. In each case the heater was operating at spark breakdown point.

Time did not allow for comprehensive investigations of the independent effects of mass flow rate and power input to be made, but the evidence shown (fig. 15) suggests that conversion efficiency increases with mass flow rate. However, the genrally low figure of 0.3-0.5 cannot be wholly accounted for by experimental errors. Most of the steady state convective losses from the exterior of the tube can be expected to be recovered in the form of an increased inlet gas temperature, and an estimation of the loss from the outlet duct indicates that this is less than about 15% for these tests. The estimation was made by the use of the assumption of a fully developed turbulent pipe flow in the duct and indicated a loss of about 5%; the factor of 3 was allowed to cater for the possibility of boundary layer, or not fully-developed flow. Since this loss would increase with Reynold's Number and hence with mass flow rate, it is evident that there must be a considerable remaining energy loss which must decrease with increasing flow rate. The most likely source of this loss is thought to be that of natural convection from within the tube set up by the inevitable temperature gradients present. The loss would be expected to decrease as the mass flow rate increased, and increase as operating temperature increased. It would be difficult to predict what the overall effect of this would be as both of these variables were increased to practical operating values; the only way to avoid the problem altogether would be to invert the whole electrode arrangement so that convection currents assisted the flow. This change would not be difficult.

5.6.2 Tests to check theoretical assumptions

Current-voltage relationship

The validity of the basic current-voltage relationship was tested by a series of measurements made with a polished copper tube of 10.1 cm diameter and cylinder ratios p_r of 142.8, 270.3, 322.6 and 400, in air at atmospheric pressure. The wires were of nickel and at positive polarity.

Measurements were made of current and voltage from corona onset to spark breakdown, and the results, plotted on the basis described in Appendix XI, are shown in fig.20, using dummy values of K_o and E_r^* of 2.00 cm^2/volt.sec. and 100kV/cm respectively. The corresponding

theoretical curves are shown in fig. 21; the fit between theoretical and experimental curves is very good, giving derived values of mobility and starting field strength as shown in fig. 20. Slight deviation is evident in all curves at high values of current, indicating a probable increase in ion mobility with increasing field strength.

Preliminary high temperature experiment

While the main equipment was being manufactured an approximate check on the breakdown assumption was made. A stainless steel tube 30 cm long and 3.1 cm diameter was fitted with a concentric wire of 0.25 mm diameter. Bungs of ceramic were inserted into each end to reduce the effects of internal convection, and the tube, mounted horizontally, was heated to a dull red glow (about 800°C) by means of gas flames. Several runs were made, both alternating and direct voltage being used, and the breakdown voltages were compared with those obtained with the unheated tube. In each case it was found that the breakdown voltage was about one third of that at atmospheric temperature, thus roughly verifying, within this temperature range, that breakdown voltage varied inversely with density.

Breakdown and starting voltages at high pressure

A series of tests was made on the heater to determine the effect of pressure on starting and breakdown voltage at atmospheric temperature. Measurements were made with a cylinder ratio of 37.4, up to a pressure of about 8 atmospheres. The starting voltage was assumed, for convenience, to be the voltage at which the current was 10 μA; the applied voltage was then raised rapidly towards the breakdown value to avoid the effects of heating. The results are shown on fig.(16). It is seen that the breakdown voltage rises only by a factor of 4 while the starting voltage appears to be almost constant. The final low figure of starting voltage was due to a partial insulation failure; this is not thought to have affected the breakdown voltage. A "conditioning" (Ref.2, p.942) of the wire was also thought to have affected the starting voltage during the tests; conditioning is a process frequently used for preparing electrode surfaces, particularly prints, prior to tests of this nature, and involves repeated sparking. The method is not suitable for wires as it could not be ensured that the whole surface was affected.

The breakdown figures illustrate the rather random nature (see chapter 4) of breakdown from a streamer mode of corona; the hiss of the streamers could be heard through the pressure vessel walls as breakdown was approached. It is not therefore thought that these values represent the upper limit to what could be achieved. Similar inconsistances were noticed in fact throughout the development programme; for one particular wire and tube at atmospheric pressure, breakdown voltages between 7kV and 17 kV were observed.

Other assumptions

Since at best only an indirect check on the overall validity of the theory could be gained from the heating experiments, some other means was sought for a check on specific assumptions. It was intended to achieve this by conducting current-voltage measurements at several values of operating pressure, with a gas mass-flow rate sufficiently high that at all power inputs the temperature rise would be small. This would ensure that the gas density was nearly uniform throughout the tube, and the results could be analysed by the method described in Appendix XI. Thus the variation of starting field strength, breakdown strength and mobility with pressure would be obtained at ambient temperature; to assess the effect of increasing temperature would be much more difficult. Owing to the development problems described in Appendix X, however, there was not time to complete these tests, only the shortened series of measurements described in the previous sections being made.

6. General Discussion

A number of assumptions was made in the theory (sections 2.1 and 2.4.1), some concerning boundary or limiting conditions, and others were introduced in order to simplify the problems for analysis. Their validity is now examined on theoretical grounds, and in the light of the experiments and those of other workers in related fields.

6.1 Simplifying assumptions

6.1.1 Coincidence of field lines

In the axial field heater analysis it was assumed that electrical and aerodynamic fields were uniform and coincident everywhere. This requirement can be met very closely at the collector station by a wire mesh screen, which acts as a good electrical earth while being permeable to air. At the emitter, however, there is the additional requirement of the ion source. The most convenient mechanism of ion production, as mentioned in the introduction, is by corona emission from a surface of high curvature. In the above context (see section 2.5) this would entail a series of fine points arranged to lie in a uniform distribution on the emitter plane. The electric field distribution and current density would therefore be very non-uniform near the points. Since the length of the heating section would have to be of the same order as the separation of the points to achieve the required highly divergent field, non-uniform conditions would prevail over a large proportion of the gap; reasonably uniform aerodynamic conditions could of course be achieved by suitable design of the emitter. Thus it would be expected that the idealised operation, with the breakdown condition obtained at the collector, would not be achieved, since breakdown streamers would almost certainly propagate from the emitter points, where a state of partial breakdown, the corona, already exists.

In the radial field case there was assumed to be no interaction between the electrical and aerodynamic fields, so that no momentum exchange took place between space charge and neutral gas. This point is further discussed in section 6.1.4.

6.1.2 Ion mobility

Throughout the axial field analysis (sections 2.2 and 2.3) and in the simplified radial field analysis (sections 2.4) it was assumed that ion mobility was inversely proportional to gas density. This has been shown by Shale and others[10] to be justifiable for positive ions in air for at least part of the range of density and field strength of interest (17 kg/m^3, 100 kV/cm). There is, however, evidence from both the present experiments (see section 5.6.2) and other sources[10,16] that mobility increases slightly at field strengths approaching breakdown values.

For the general analysis of the radial field heater the mobility was left as an arbitrary function of temperature and pressure; in the example computed it was taken as proportional to local density. Any further generalisation (e.g. to allow for variation with field strength) would make analysis very complicated and was thought not justified at this stage.

6.1.3 The energy equation

The assumption implicit in the use of the energy equation in the form of equation (1.3) is that all losses are small. Two sources of loss are those of dissociation and ionisation within the corona region. Now the dissociation potential of either nitrogen or oxygen is of the same order as the ionisation potential; thus, since the current in the corona region is the same as that in the remainder of the gap, an approximate criterion for both of these losses to be small is that V_I/V_2 is small, where V_I is the first ionisation potential and V_2 the applied voltage. Since V_I is of order 10 volts and V_2 of order 10 kV in practice this requirement is satisfied. Another energy loss is that of each ion on its terminal impact at the collecting surface; this should be small if the ratio λ/d is small, where λ is the ion mean free path, and d the electrode gap length, which is also satisfied.

A more serious source of heat loss from the radial field heater is by convection, both directly by hot gas issuing from the "inlet" to the heater tube (see section 5.6.1) and indirectly from the exterior of the tube.

The neglect of these losses was purely for convenience of analysis, although it is thought that the latter could be made indefinitely small either by insulating the exterior of the tube or by suitably ducting the convected gas to the intake to achieve a regenerative heating process. The former, as suggested in section 5.6.1, could be eliminated by inverting the heater.

Heat losses by convection from an axial heater would be considerable (see section 2.5) unless well lagged; such a heater would have considerable thermal inertia necessitating long "warming up" periods before operation.

6.1.4 The strip theory (radial heater)

In order to apply the strip theory used in assessing heater performance (section 2.4.2) it was necessary to assume that the gas temperature and axial velocity were uniform across the tube at any section, and that there was no mutual interference of any sort between adjacent elements.

Neither of the two uniformity requirements is likely to be closely met in practise, since the energy distribution from the discharge is not uniform, being much greater near the wire, and because of viscous and convective forces on the gas. It is thus unlikely that the theory gives an accurate detailed description of the heating process. However, there are processes at work within the gas, including the above, which would give mixing on a larger scale. The others are: the very small effect of molecular diffusion arising from density gradients; and forced convection by virtue of electrical body forces acting radially. The latter effect is thought to be quite considerable, as the pressure difference across the gap can be shown to be (see Appendix XII) $\Delta p = p_{R_1} - p_{r_0} = \epsilon \psi \ln \frac{R_1}{r_0} \doteq \epsilon \eta \frac{V_2^2}{R_1^2} \ln p_r$ (using previous nomenclature). As a numerical example, suppose that $V = 80$ kV, $R = 1.4$ cm., $p_r = 100$ and η = unity; then $\Delta p = 0.125$ atmospheres. Thus the average radial body force is at least an order of magnitude greater than the axial aerodynamic force. Measurements made downstream of "mixed field" and radial field electrodes at atmospheric pressure [1] (ref. 1) showed that both velocity and temperature were reasonably uniform across the duct, suggesting substantial mixing.

Thus while it would be very difficult to allow for these mixing processes in the theory, or even to make comparative assessments of them, their total effect should be to reduce the temperature gradients caused by the discharge. Hence the overall performance of the heater may not show significant variation from that predicted, if losses were accounted for. Mutual electrical intereference between elements is thought to be small provided $dR_1/d\ell$ is small; for the electrical and magnetic forces imposed on the space charge by the adjacent space charge and its motion are both very small compared with the force imposed by the applied field. This can easily be shown by an order-of-magnitude estimation of the wire current needed to produce an appreciable effect.

6.1.5 Electrical conductivity of gas

An assumption used throughout the theory is that gas conductivity is negligible; a more general form of the energy, momentum, mobility and Poisson's equation should allow for a finite proportion of free electrons and negative ions. The perfect gas law will also cease to hold with a gas of finite conductivity, especially in the case of a diatomic gas, in which there will also be substantial dissociation.

The critical operating temperature, at which the current-voltage relationship will be affected, will be very high (say above $2000^{\circ}K$)[17], and will depend not only on the pressure but also on the applied voltage, since thermal ionisation will be assisted by the small proportion of high energy ions of the dark discharge. It would also be expected that for the cylindrical electrode system, the region immediately surrounding the wire would be affected first, owing to temperature and ion energy gradients.

The onset of substantial ionisation would probably coincide with an instability of operation, owing to the consequent rapid rise in current; the discharge would then tend to become an arc. This point thus probably marks the limit of usefulness of this form of heating.

6.2 Boundary conditions

For the axial field heater the only applied boundary condition was that an assumed critical field E_o was required at the emitter station. As was implied in section 6.1.1, this is a gross simplification of the real situation, but appeared to yield results consistent with experiment at atmospheric pressure[1]. The assumed linear variation of E_o with density is thought unlikely to hold exactly. An implicit extra requirement is that no wall boundary condition need be applied; the insulating wall of duct between the electrodes will collect charge, but the effect of this will be small provided the length/diameter ratio of the heating section is small (see section 2.5).

The electrical boundary condition applied for the radial heater was that a critical field E_r^* was required at the wire surface for corona emission, regardless of current. Although again this is a simplification, it appears largely justified by the results. There is, however, ample evidence[18] that E_r^* is dependent on wire radius, or more properly, on local field distribution, with the implication that it is not a function of gas properties alone; thus more experimental evidence would be needed to ensure its correct use with the heater performance computer programs.

6.3 Terminal condition: spark breakdown

The upper limit to heater performance is controlled by the spark breakdown condition, whereby the gas between the electrodes suddenly becomes conducting in a very narrow zone. If the external circuit permits, the spark will develop into an arc. This, however, is usually prevented in the case of direct voltage, as the high tension source is smoothed by a capacitor which is partially discharged when a spark passes, thus momentarily lowering the voltage across the gap to below the sparking value. It would thus be technically possible to operate at or above the breakdown voltage, with a frequency of sparks set by an overall time constant, but this would have the following disadvantages:

1. Much of the energy in the sparks would be transferred to the electrodes rather than the gas.

2. Erosion of the electrodes, particularly the emitter, would be caused by the sparks, which would affect both performance and reliability.

Both of these are also problems encountered with the method of arc heating, which it was the intention of the present method to avoid.

The breakdown criterion used in the axial heater analysis was the relationship equation 4.5 of chapter 4, together with the experimental observation[19] that for plane parallel electrodes within the range of interest, breakdown voltage is directly proportional to both pressure and gap length at normal temperatures. Thus since the space charge is negligible before sparking the field strength is proportional to density over this region (up to about 8 atmospheres). The limitations of this assumption in practice have already been pointed out in section 6.1.1. It is also probable that gas temperature has an independent effect on breakdown, although this may be small below 500°C.

For the radial heater a similar concept was used, the assumption being that the voltage/gap ratio (ignoring wire radius) at breakdown was dependent only gas temperature and pressure. In the simplified case a linear relationship with density was assumed, as for plane parallel electrodes. Since the field strength at a given radius is not directly proportional to voltage, owing to the space charge, this is a simplification, although if the voltage is sufficiently high the field tends towards uniformity (see section 2.4.2) which redeem the situation to some extent.

As in the axial field case, however, the concept of a "breakdown field strength" or similar is inadequate to deal completely with the real situation; for a state of partial breakdown already exists, and the question is one of propagation from that state. This depends as much on distribution of field strength as on its magnitude at any given point, as the work of Uhlig[4], Uhlmann[20], and others has shown. The point is best illustrated by means of a diagram[21] of applied voltage versus r_o/R_1, or $1/p_r$, as shown; the diagram is due to Uhlmann.

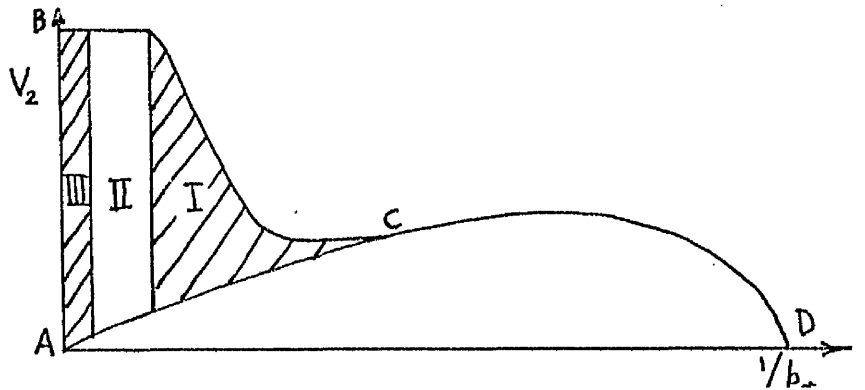

If the voltage is below the line ACD no discharge can occur; between A and C this line represents the locus of the corona starting voltage. Instantaneous spark breakdown occurs above the limit line BCD. Corona can exist, therefore, within the region ABC. Consider, for convenience, a fixed outer cylinder of radius R . Then for a very small r_o (region III), the corona is in phase III of section 3.3 , and breakdown can occur anywhere within it, with the probability increasing as voltage is raised. Within region II, for a slightly greater r_o, the "burst pulse" corona of phase II is obtained, and according to Uhlig[22], the breakdown voltage becomes very well defined and only occurs at the upper limit to the region. The final zone I, denotes the streamer phase (phase I) of corona, in which a spark can occur at any voltage between the limit lines AC and BC.

The above is again a very simplified picture; the boundaries between the regions are not well defined, and are dependent on other parameters such as gas temperature, and the ratio r_o/λ. The former effect will become manifest in thermal ionisation, while the latter is exemplified by the fact that Uhlig's experiments revealed "burst pulse" corona from starting voltage up to breakdown for a cylinder ratio p_r of about 300, while in control experiments in the present programme this form was not observed at any voltage, although the cylinder ratio was similar. The main reason is thought to be that the scale was different; the value of the parameter r_o/λ in Uhlig's experiments was about 10^5, while in the present experiments it was about 10^3. Other factors such as dust and water vapour content of the gas may also be significant.

The geometry of the heater investigated here was also such that the corona was in the streamer phase (III), with consequent random breakdown voltage; attempts to obtain burst-pulse corona by altering the cylinder ratio and by other means (see section 5.5.3) were not successful. As was reported earlier, Hermstein[5] has shown that burst pulse corona can be initiated and maintained by an external control mechanism; if such could be introduced, there is some reason to believe that the assumed breakdown condition may be approached, as Uhlig[4] reported a breakdown voltage directly proportional to electrode gap with this phase.

7. Conclusions

A theoretical analysis of the two basic heater geometries, coupled with practical arguments based on preliminary experiments, showed that the radial field arrangement was preferable. The theory was developed to predict the performance of both a constant radius heater and for an "optimum" shape, in which a condition near to spark breakdown was maintained over the whole length. A modification was also given for the use of alternating voltage, for which it was shown that the power input for a given peak voltage V_a could not exceed $4/3\pi$ of that for a direct voltage V_2.

A constant radius heater designed to a simplified theory achieved an indicated maximum performance of a flow rate of 1.25 gm/sec. of nitrogen with a temperature rise of $87^{o}C$, at a conversion efficiency of 0.45. The designed performance was not attained for the following reasons:

1. Development problems prevented operation at the maximum voltage available.
2. Heat losses were greater than expected.
3. The spark breakdown condition assumed was optimistic.
4. The theoretical model was incomplete.

Methods of controlling heat losses have been suggested, but much more fundamental experiment would be required before a reliable breakdown criterion could be given. Some form of external control mechanism on the corona discharge may be necessary if reliable performance is to be ensured with the present scale of apparatus.

In view of the limited experimental results a direct check on the validity of the method of analysis (the strip theory) was not possible, although the basic current-voltage relationship was justified.

Operation of the equipment with alternating voltage is not recommended at this stage, partly for theoretical reasons and partly since, with the power available from a transformer, very fast trip mechanisms would be needed to prevent the wire electrode being fused by the arc in the event of gas breakdown.

With present knowledge no definite conclusion can be reached as to whether a heater suitable for a high enthalpy wind tunnel can be made on this principle. The results indicate, however, that an efficiency of energy transfer can be obtained which is substantially higher than that typical of arc heating, suggesting that the work would repay further attention. The greatest problem remaining is that of controlling and predicting spark breakdown, which involves more fundamental work on the discharge process; the corona discharge in the range of pressure, voltage, and dimensions peculiar to this application has not been previously studied in detail.

Acknowledgments

The author wishes to thank the following:

Professor T.R.F. Nonweiler, of the Department of Aeronautics and Fluid Mechanics, and Dr. T.R. Foord, of the Department of Electrical Engineering, for their advice and encouragement during the project;

Mr. R.R. Perry, who constructed the apparatus and gave invaluable assistance with the experiments;

Mr. R. Cowper, of the Department of Fine Arts, who developed the photographic plates and prepared the enlargements.

The work was supported by the Ministry of Technology under contract number PD/48/05.

References

1. J.E. Hesselgreaves, T.R.F. Nonweiler and T.R. Foord. "The heating of air by 'dark' discharge" ARC R & M No. 3519 1967.

2. L.B. Loeb. "Basic Processes in Gaseous Electronics" (Book). University of California Press. 1961.

3. C.G. Miller, L.B. Loeb. "Positive coaxial cylindrical corona discharges in pure Nitrogen, oxygen and mixtures thereof". J. Appl. Phys. vol. 22, no.5, p.494, April 1951.

4. C.A.E. Uhlig. "The ultra corona discharge, a new discharge phenomenon occurring on thin wires". Proc. High Voltage Symposium, Paper 15, Nat. Res. Council, Canada. September 1956.

5. W. Hermstein. "Die Stromfaden-Entladung und ihr Übergang in das Glimmen" Archir für Elektrotechik Vol.45, No.3, 1960.

6. M. Robinson. "Movement of air in the electric wind of the corona discharge". Trans. AIEE, Vol.81, p.143, 1961.

7. Stuetzer. "Ion drag pressure generation". J. Appl. Phys. Vol. 30, p. 984, 1959.

8. A. Marks, E. Barreto and C.K. Chu. "Charged aerosol energy converter". AIAA Journal Vol. 2, no. 1, p. 45. 1964.

9. M.C. Gourdine, E. Barreto and M.P. Khan.
"The performance of electrogasdynamic generators" Appendix D, Internal Report, Wright Aeronautical Division, Curtis-Wright Corporation. Wood-Ridge, N.J. 1965.

10. C.C. Shale. "The physical phenomena underlying the negative and positive coronas in air at high temperatures and pressures". IEEE International Convention Record 1965 part 7.

11. A.H. Shapiro and W.R. Hawthorne.
"The mechanics and thermodynamics of steady, one-dimensional gas flow". Jnl. Appl. Mech. Trans ASME, Vol.14, No.4, p.317. 1947.

12. T.R.F. Nonweiler. "Electrostatic accelerators as energy sources for supersonic intermittent tunnels". Unpublished report, University of Glasgow 1962.

13. J.S. Townsend. "Electricity in Gases" (Book). Oxford University Press, 1914.

14. L.B. Loeb. "Recent developments in analysis of the mechanisms of positive and negative coronas in air". J. Appl. Phys. Vol. 19, no. 10, p.882, 1948.

15. L.B. Loeb. "Statistical factors in spark discharge mechanisms". Rev. Mod. Phys., Vol.20, No.1, p.151.

16. J.M. Meek, and J.D. Craggs.
"Electrical breakdown of gas" (Book) Clarendon Press, Oxford 1953.

17. D.W. George. "Sources of ionisation in high pressure gases above 2000^{o}K". Proc. IEE, Vol.III, No.9, September 1964.

18. J.D. Cobine. "Gaseous conductors: theory and engineering applications" (Book). Dover, New York 1959.

19. E.R. Cohen. "Electric strength of highly compressed gases". Proc. IEE, Vol.103, part A.

20. E. Uhlmann. "Der Elektrische Durchschlag von Luft zwischen Konzentrischen Zylindern". Archiv für Elektrotechnik Vol.23, p.323, 1929.

21. C.A.E. Uhlig. "A.C Corona current and loss on thin wires from onset to sparkover". Proc. High Voltage Symposium. Paper 16, Nat. Research Council, Canada. 1956.

Appendix I

Derivation of equations 1.17 and 1.20

Equation 1.17

The dimensionless temperature increment dT/T is found by eliminating p, q and ρ between equations 1.1, 1.2, 1.3 and 1.4 as follows:

Equation 1.3 may be rewritten

$$\frac{dT}{T} + (\gamma-1)M^2\frac{dq}{q} = -j\frac{Q_0\,dV}{C_pT} \quad . \qquad \text{II.i}$$

From equations 1.1, 1.2, 1.4, dT/T becomes

$$\frac{dT}{T} = \frac{dp}{p} - \frac{d\rho}{\rho} = -\frac{\alpha\rho Q_0\,dV}{p} - \gamma M^2\frac{dq}{q} + \frac{dq}{q} + \frac{dA}{A}$$

$$= -\frac{\alpha\rho Q_0\,dV}{p} - \frac{(1-\gamma M^2)}{(\gamma-1)M^2}\left[j\frac{Q_0\,dV}{C_pT} + \frac{dT}{T}\right] + \frac{dA}{A} \quad .$$

By rearrangement and simplification

$$\frac{dT}{T} = -j\frac{Q_0\,dV}{C_pT}\left(\frac{(\gamma-1)M^2}{1-M^2}\right)\left[\frac{1-\gamma M^2}{(\gamma-1)M^2} + \frac{\alpha}{j}\cdot\frac{\gamma}{\gamma-1}\right] + \frac{(\gamma-1)M^2}{1-M^2}\cdot\frac{dA}{A}$$

$$= -\frac{jQ_0\,dV}{C_pT(1-M^2)}\left[1 - \gamma M^2\left(1 - \frac{\alpha}{j}\right)\right] + \frac{(\gamma-1)M^2}{1-M^2}\cdot\frac{dA}{A} \quad .$$

By substitution of equation 1.14 in the main text equation 1.17 is obtained:

$$\frac{dT}{T} = \frac{dW}{(1-M^2)}\left[1 - \gamma M^2\cdot\frac{u}{u+1}\right] + \frac{(\gamma-1)M^2}{1-M^2}\cdot\frac{dA}{A} \quad . \qquad 1.17$$

The remaining equations 1.15, 1.16, 1.18, 1.19 are obtained in a similar way, using equation 1.17.

Equation 1.20

Poisson's equation (1.12) is

$$\frac{dE}{E} + \frac{dA}{A} = \frac{\alpha \rho Q_o d\ell}{E\epsilon}$$

$$= \frac{i\, d\ell}{E.q\epsilon A(u+1)} \qquad \text{I.ii}$$

from equations 1.9 and 1.14.

But $d\ell = \frac{dV}{E}$, from equation 1.11, and

$u = \frac{\rho_o k_o E}{\rho q}$, from equations 1.8 and 1.14, from which

$$u = \frac{\rho_o k_o}{\dot{m}} . AE . \qquad \text{I.iii}$$

Since ρ_o, k_o and $\dot{m}$ are constants within a streamtube or tube of force, differentiation of equation iii gives

$$\frac{du}{u} = \frac{dA}{A} + \frac{dE}{E} . \qquad \text{I.iv}$$

Thus equation ii becomes

$$\frac{du}{u} = \frac{i\, dV}{E^2.q\epsilon A(u+1)} ,$$

which, by equations (iii) and (1.13) in main text, becomes, after rearrangement,

$$(u^3+u^2)\frac{du}{u} = dW. \frac{\rho_o k_o^2}{\epsilon} . \frac{\rho_o}{\rho} . \frac{1}{M^2(\gamma-1)} . \qquad 1.20$$

Appendix II

Axial field heating at low Mach Number

i. Temperature rise

The only quantities in equation 2.1 which change from emitter to collector are T and E, so the equation may be integrated to give the temperature in terms of the field strength at any station in the duct:

$$\ln\left(\frac{T}{T_o}\right) = \frac{\epsilon A k_o E^3}{3 \dot{m} C_p T_o n}\left(1 - \frac{E^{*3}}{E^3}\right) \qquad \text{II.i}$$

where E^* is the field at the emitter required to produce corona emission (see discussion in section 6.2), and is assumed to be independent of current.

Now, as in section 2.2, the simplest breakdown condition applicable is that E/ρ has a maximum permissible value; the heater will operate in its optimum condition when this value is obtained at the collector, where the field is highest. The condition may be expressed as

$$E_c = E_{b,a} \cdot n \frac{T_o}{T_c} \quad , \qquad \text{II.ii}$$

where suffix c refers to the collector, and $E_{b,a}$ is the breakdown strength pertaining to the geometry at atmospheric conditions. Substitution of equation II.ii into II.i then gives equation 2.2 in the main text:

$$\left(\frac{T_c}{T_o}\right)^3 \ln\left(\frac{T_c}{T_o}\right) = B_b \cdot n^3\left(1 - \frac{E^{*3}}{E_c^3}\right) \quad , \qquad 2.2$$

where $$B_b = \frac{\epsilon A k_o E_{b,a}}{3 \dot{m} C_p T_o n} \quad .$$

If it is assumed that the starting field E^* is dependent on gas density as is E_c, equation 2.2 may be rewritten:

$$B_f n^3 \left(\frac{T_o}{T_c}\right)^3 - \ln\left(\frac{T_c}{T_o}\right) = B_f n^3 \left(\frac{E_o}{E_f}\right)^3 \quad , \qquad \text{II.iii}$$

where $E_o = E^*/n$, and is the starting field at atmospheric conditions.

ii. Length of heater

The combination of equations 1.10, 1.2, 1.14 and 1.18 gives

$$d\ell = \frac{\dot{m} C_p dT}{i E} \quad , \qquad \text{II.iv}$$

and since (from equation II.i)

$$E = \frac{E^*}{B_o^{1/3}} \left(\ln\left(\frac{TD}{T_o}\right)\right)^{1/3} , \qquad \text{II.v}$$

where $B_o = \dfrac{\epsilon A k_o E^{*3}}{3 \dot{m} C_p T_o n}$, and $D = \exp(B_o)$,

substitution into equation II.iv gives, upon integration, the length of the heater in terms of the temperature rise:

$$L = \frac{\dot{m} C_p B_o^{1/3} T_o}{i E^*} \int_1^{T_c/T_o} \frac{d(T/T_o)}{(\ln(TD/T_o))^{1/3}} \quad . \qquad \text{II.vi}$$

This expression can be simplified by the integration of 1.18 together with 1.10:

$$\dot{m} C_p (T_c - T_o) = iV \qquad \text{II.vii}$$

and the use of equation II.v referred to the collector:

$$E_c = \frac{E^*}{B_o^{1/3}} \left(\ln\left(\frac{T_c D}{T_o}\right)\right)^{1/3} . \qquad \text{II.viii}$$

Substitution of these equations gives equation 2.4 in the main text :

$$L = \frac{V}{n E_b} \cdot \frac{1}{1 - T_o/T_c} \int_1^{T_c/T_o} \left(\frac{\ln\left(\frac{T_c D}{T_o}\right)}{\ln\left(\frac{T D}{T_o}\right)} \right)^{1/3} d\left(T/T_o\right) \qquad 2.4$$

The length to diameter ratio of the heating section is an important parameter (discussed in section 2.5) and is obtained from equations 2.4 and 2.2. It may be expressed as

$$\frac{L^2}{R^2} = \frac{\pi V^2 \epsilon k_o E_b}{3 \dot{m} C_p T_o} \left\{ \frac{I}{(1 - 1/t_c)^2 \cdot t_c^3 \ln(t_c D)} \right\} , \qquad \text{II.ix}$$

where $$I = \int_1^{t_c} \left(\frac{\ln(t_c D)}{\ln(tD)} \right)^{1/3} dt ,$$

and $t = T/T_o$, t_c referring to the collector.

Appendix III

Current-voltage relationship for radial field

Poisson's equation in the form for radial symmetry is (c.f. equation 1.7)

$$\frac{1}{r}\frac{d}{dr}(rE_r) = \frac{\alpha\rho Q_o}{\epsilon} \quad , \qquad \text{III.i}$$

where E_r is the radial field strength; other parameters are as in section 2.2. The equation of conservation of charge is:

$$\frac{di}{dl} = 2\pi r\alpha v_r \rho Q_o \quad \text{(independent of r)}, \qquad \text{III.ii}$$

where i is the current and v_r is the radial drift velocity of ions. The mobility equation is

$$v_r = kE_r \quad . \qquad \text{III.iii}$$

The quantities $\alpha\rho Q_o$ and v_r can now be eliminated from III.i and III.ii, giving

$$\frac{d}{dr}(rE_r) = \frac{di/dl}{2\pi\epsilon k} \cdot \frac{1}{E_r} \quad . \qquad \text{III.iv}$$

By assumption (c) in the main text put

$$\psi = \frac{di/dl}{2\pi\epsilon k} \quad . \quad \text{(independent of r)}. \qquad \text{III.v}$$

Equation III.iv may now be integrated to give

$$E_r^2 = \psi + \frac{\phi^2}{r^2} \quad , \qquad \text{III.vi}$$

where ϕ is a constant of integration. When the current is zero this equation may be integrated again to give the familiar logarithmic voltage distribution (c.f. equation 3.7 in main text). To account for a

finite current appropriate boundary conditions must be applied to find ϕ, the most widely accepted one being that a minimum field E_r^* is required at the wire surface ($r = r_o$) for corona to be established there. This field is assumed to be independent of current.

Thus $$E_r^{*2} = \frac{\phi^2}{r_o^2} + \psi \quad ,$$

giving $$\frac{\phi^2}{\psi r_o^2} = \frac{E_r^{*2}}{\psi} - 1 = \frac{1}{X^2} \quad \text{(say)}. \qquad \text{III.vii}$$

Equation III.vi then becomes

$$\frac{dV}{dr} = \pm \psi^{1/2}\left(1 + \frac{r_o^2}{r^2 X^2}\right)^{1/2} \quad , \qquad \text{III.viii}$$

which upon integration yields the voltage distribution

$$\frac{V(r)X}{\psi^{1/2} r_o} = \pm\left[\left(1 + \frac{r^2X^2}{r_o^2}\right)^{1/2} - \left(1+X^2\right)^{1/2} - \operatorname{cosech}^{-1}\frac{Xr}{r_o} + \operatorname{cosech}^{-1}X\right]. \qquad \text{III.ix}$$

Suppose that the applied voltage is V_a at the emitter (wire), positive with respect to the outer cylinder, which is earthed. A positive space charge is then obtained, and substitution of this condition then gives, on re-arrangement,

$$\frac{V_a X}{\psi^{1/2} r_o} = \left(1 + X^2 p_r^2\right)^{1/2} - \left(1+X^2\right)^{1/2} + \ln p_r + \ln\left(\frac{1+(1+X^2)^{1/2}}{1+(1+X^2p_r^2)^{1/2}}\right), \qquad 3.1$$

where $p_r = R_1/r_o$.

Small-current approximation

If the current is so small that $X^2 p_r^2 \ll 1$, equation 3.1 can be expanded to give

$$\frac{V_a X}{\psi^{1/2} r_o} = \ln p_r + \frac{\psi}{4E_r^{*2}}\left(p_r^2 - 1\right), \qquad \text{III.x}$$

or $$\frac{V_a}{E_r^* r_o} = \ln p_r + \frac{\psi}{4E_r^{*2}}\left(p_r^2 - 1\right),$$

which, by reference to equations 3.3 and 3.7 in the main text, can be expressed as

$$\frac{di}{d\ell} = \frac{(V_2 - V_0).8\pi V_0 \epsilon k_0}{R_1^2(1-\beta_r^2)\ln\beta_r} . \qquad \text{III.xi}$$

The range of voltage over which this equation is applicable is found by rewriting it as:

$$\psi = \frac{4V_0^2 \ln\beta_r}{R_1^2(\ln\beta_r)^2}\left(\frac{V_2}{V_0}-1\right).\frac{r_0^2}{r_0^2} = \frac{4r_0^2 E_r^{*2}\ln\beta_r}{R_1^2}\left(\frac{V_2}{V_0}-1\right),$$

giving the condition $X^2\beta_r^2 \ll 1$ as

$$\frac{\psi R_1^2}{E_r^{*2} r_0^2} = 4\left(\frac{V_2}{V_0}-1\right)\ln\beta_r \ll 1 . \qquad \text{III.xii}$$

Appendix IV

Constant radius heater: calculation of η

As stated in section 2.4.4, η is found by the formation of the variable X and the use of equation 3.6.

The basic current-voltage relationship is (equations 3.3 and 3.5):

$$\Psi = \frac{\eta V_2^2}{(1-1/p_r)^2 R_1^2} = \frac{\eta}{(1-1/p_r)^2} \cdot E_{b,r}^2 \cdot E_m^2(n, T_f/T_o). \qquad \text{IV.i}$$

Suppose now that the critical wire surface field strength, E_r^*, is dependent on local gas temperature and pressure such that

$$E_+^* = E_{o,+} \cdot E(n, T_\ell/T_o), \qquad \text{IV.ii}$$

where $E_{o,r}$ is the critical field strength at atmospheric conditions (note that E_r^* and $E_{o,r}$ correspond to E^* and E_o of section 2.3 and Appendix II).

Division of equation IV.i by the square of equation IV.ii now gives

$$\frac{\Psi}{E_+^{*2}} = \frac{\eta}{(1-1/p_r)^2} \cdot \left(\frac{E_{b,r}}{E_{o,+}}\right)^2 \cdot \frac{E_m^2(n, T_f/T_o)}{E^2(n, T_\ell/T_o)}. \qquad \text{IV.iii}$$

Thus, for a local temperature T_ℓ and known final temperature T_f, Ψ/E_+^{*2} can be found in terms of η, whence

$$X^2 = \frac{\Psi/E_+^{*2}}{1-\Psi/E_+^{*2}}. \qquad 3.2$$

Now since the cylinder ratio p_r is known, examination of equations IV.iii, 3.2 and 3.6 shows that 3.6 may be written

$$\eta = f(\eta), \qquad \text{IV.iv}$$

which is solved by guessing a starting value and using the simple expression $\eta_{n+1} = f(\eta_n)$, it being known that η is a well-behaved function of X.

Appendix V

Algol procedures used for solution of heating equations (radial field heaters)

(i) Constant radius heater

Description of procedures.

The principal procedure is procedure "conheat", which perform the integration of the temperature increments along the heater as described in section 2.4.4 of the main text. Three functions "E_m", "K" and "E" are called by "conheat" to provide the dependence of breakdown field, mobility and starting field on pressure and temperature. In the examples E_m and E are given as being directly proportional to density, while K is inversely proportional to density. A procedure "result", one of the formal parameters of "conheat", provides current answers as required (e.g. local temperature, length, η), and the final answer at the required exit temperature. All parameters are dimensionless.

```
real procedure Em(atm,temp); value atm, temp; real atm, temp; Em:= atm/temp;
real procedure K (at ,tem); value at, tem; real at, tem; K := tem/at;
real procedure E (a,te); value a,te; real a,te; E = a/te;
procedure conheat (pt,dx,r,tf,n,Bl, result)
value pt,dx,r,tf,n,Bl; real pt,dx,r,tf,n,Bl; procedure result;
begin comment pt is cylinder ratio, dx is increment of length,
      r is ratio of corona field to breakdown field, tf is required
      temperature ratio (output/input), n is the pressure in atmospheres,
      Bl is a parameter (see equation 3.15), and "result" is the output
      procedure providing, for example, temperature and length, depending
      on a counter;
      comment breakdown occurs at end of tube at temperature t ;
      real Xsqd,lnpr,s,t,eta,S,Sl,tx,dt,Ef,DX; integer i,j;
      tx := 1.0; eta := 0.4; S := eta; i := 0; lnpr := ln(pr);
      Ef := Em (n,tf); DX := dx x Bl x Ef;
      for i := i + 1 while tx < tf do
```

```
        begin comment first iterate to find eta;
            A:  S1 := S;
                Xsqd := 1.0/((r x E(n,tx)x(1.0-1.0/p↑)/E_m(n,t ))↑ 2.0/eta-1.0);
                s := sqrt(1.0+Xsqd x p↑ x p↑);  t := sqrt(1.0+Xsqd);
                eta := Xsqd x ((p↑-1.0)/(s-t+ℓnpr+ℓn((1.0+t)/(1.0+s))))↑ 2.0;
                S := eta;
                if  abs(1.0-S/S1)> 10-3 then goto A;
                dt := DX x K(n,tx) x eta/(1.0-1.0/p↑); tx := tx + dt;
                result (temp,length,counter);
                j := i;
        end;
        result (temp,length,counter);
end     conheat ;
```

(ii) Optimum shape heater

Description.

The only difference between this procedure "optheat" and procedure "conheat" is that the cylinder ratio and radius are variable; thus the starting cylinder ratio $p\uparrow s$ is used as a formal parameter instead of $p\uparrow$. The functional procedures E_m, K and E are the same, while procedure "result" will provide the radius in addition to temperature and length.

```
procedure optheat (p↑s,dx,r,tf,n,B2, result)
value p↑s ,dx,r,tf ,n,B2;  procedure result; real p↑s,dx,r,tf ,n,B2;
begin comment  p↑s  is starting cylinder ratio, dx is increment of length,
      r is ratio of corona to breakdown field, tf  is required exit
      temperature, n is operating pressure in atmospheres, B2 is a
      parameter (equation 3.18), and 'result' is an output procedure
      providing, for example, length, temperature and radius;
      comment breakdown condition is maintained over whole length of heater;
      real Xsqd,ℓnpr,s,t,eta,S,S1,tx,dt,p↑,DX;  integer i,j;
      p↑ := p↑s; tx := 1.0; eta := 0.6; S := eta; i := 0; DX := B2 x dx x E_m(n,1
      for  i := i + 1  while tx < tf  do
```

```
begin comment first iterate to find eta;
        ℓnpr := ℓn(pr);
    A:  S1 := S;
        Xsqd := 1.0/((r x E(n,tx)x(1.0-1.0/pr)/E_m(n,tx))↑2.0/eta-1.0);
        s := sqrt(1.0+Xsqdxp↑2.0); t := sqrt(1.0+Xsqd);
        eta := Xsqd x((p↑-1)/(s-t+ℓnpr+ℓn((1.0+t)/(1.0+s))))↑2.0;
        S := eta; if abs(1.0-S/S1)<10-3 then goto A;
        dt := K(n,tx)xDXxetax(E_m(n,tx))↑2.0;  tx := tx + dt;
        pr := prs x n/E_m(n,tx);
        result (temperature, radius, length, counter); j := i;
    end;
    result (temperature, radius, length, counter);
end optheat;
```

Appendix VI

Summary of nomenclature of field strengths

Consider the diagrams depicting the two geometrical arrangements:

Axial field

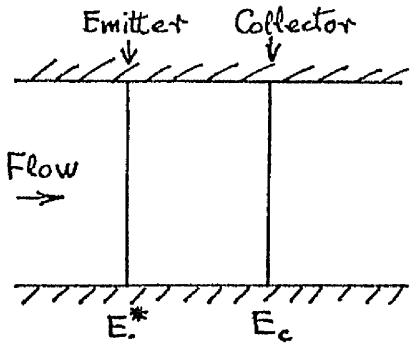

$$E^* = n E_{o,a}$$

$$E_c = E_{b,a} \cdot \frac{n T_o}{T_c}$$

Radial field

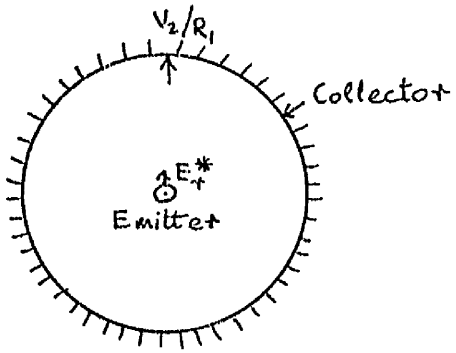

$$E_r^* = E_{o,r} \cdot E\left(n, T_e/T_o\right)$$

$$\left(V_2/R_1\right)_{B.r.} = E_{b,r} \cdot E_m\left(n, T_e/T_o\right)$$

Although the field strengths referred to have all denoted a breakdown condition in some form, that is, corona formation in one sense and spark breakdown in another, none of them will in general be identical with any other, since the concept of a breakdown field strength (see chapter 4) is inadequate for the description of more than a restricted range of practical situations. Thus the use of different suffices is necessary.

Axial fields

Current is assumed to flow when the field at the emitter plane is E^*; for the purposes of the simplified analysis this field is assumed to be proportional to density, and is thus written $E^* = nE_{o,a}$, where n is the pressure in atmospheres and $E_{o,a}$ is the starting field at atmospheric conditions. It is assumed that the temperature at the emitter is atmospheric.

At the collector the field E_c, which ideally is greatest here (by virtue of Poisson's equation), is assumed to be at breakdown point. The breakdown field is also assumed to be proportional to density, so that $E_c = E_{b,a} \cdot \frac{n T_o}{T_c}$, where $E_{b,a}$ is the breakdown field strength at atmospheric conditions, and T_c is the exit temperature.

Typical approximate values of fields from the atmospheric experiments (Ref. 1) are 2 kV/cm and 10 kV/cm for $E_{o,a}$ and $E_{b,a}$ respectively.

Radial fields

The critical field for emission (at the wire) is E_r^*, which is assumed to be a function of temperature and pressure, such that $E_r^* = E_{o,r} \cdot E(n, T/T_o)$ where $E_{o,r}$ is the normalised, or atmospheric value, and E is a dimensionless function of n and T (see section 2.4.4).

The limiting condition for the radial field is not set by the collector field but by the breakdown voltage (see section 6.3); the voltage/gap ratio at breakdown, which is used as the criterion, is given approximately by $(V_s/R_1)_{Br}$, and is expressed as

$$\left(\frac{V_2}{R_1}\right)_{Br} = E_{b,r} \cdot E_m(n, T_e/T_o)$$

where $E_{b,r}$ is the ratio at which breakdown occurs at atmospheric conditions, and E_m is another dimensionless function of pressure and temperature.

Appendix VII

An approximate criterion for the applicability of the alternating voltage analysis

The requirement may be defined as the necessity that the mean time taken for an ion to cross the gap be very much smaller than the time taken for reversal of the voltage.

For direct voltage the time taken for the ion to cross the gap is

$$t_i = \int_{r_0}^{R_1} \frac{dr}{v_r} = \int_{r_0}^{R_1} \frac{dr}{kE_r} = \frac{nT_0}{k_0 T} \int_{r_0}^{R_1} \frac{dr}{E_r} \quad ,$$

where T and n are the gas temperature and pressure respectively. Both are assumed to be independent of radius. Now make the pessimistic assumption that the field strength is everywhere equal to $\psi^{1/2}$ (see equation III.viii). Thus

$$t_i \doteq \frac{nT_0}{k_0 T} \int_{r_0}^{R_1} \frac{dr}{\psi^{1/2}} = \frac{nT_0(R_1 - r_0)}{k_0 T \psi^{1/2}} \quad .$$

Putting η = unity for simplicity this becomes

$$t_i \doteq \frac{nT_0 R_1^2}{k_0 T V} \quad ,$$

where V is the direct voltage. Now, considering an alternating voltage, and bearing in mind that most of the current passes when the voltage is near its peak value, an approximate mean time may be given as mean

$$t_i = \frac{nT_0 R_1^2}{k_0 T V_2} \quad ,$$

where V_2 is the peak voltage. Now an ion liberated at the wire near the time of peak voltage has $\frac{1}{4}$ of a cycle to cross the gap before the field is reversed, that is a time $\pi/2\omega$. Thus the criterion becomes

$$\frac{n T_o R_1^2 \cdot 2\omega}{\pi k_o T V_2} \ll 1$$

As an illustration, if the peak voltage is close to the breakdown value and the frequency is 50 Hz this sets a limit on the tube radius such that $R_1 \ll 600$ cm., which is clearly satisfied with the present apparatus.

Appendix VIII

Alternating voltage correction for radial field heater

As stated in section 2.4.6 it is assumed that the supply voltage is sinusoidal so that $V_i = V_2 \sin\omega t$, where ω is the angular frequency. Since the complete analysis requires a numerical process, it will be useful to apply two simple approximations which will yield an indication of the values of $\eta_{a.c.}$ to be expected.

Case 1. $\eta_{d.c} = 1 - V_o/V_i$

Inspection of fig.(1) shows that this approximation to $\eta_{d.c.}$ is fairly close for values of p_r of about 200 and above, which represent the upper limit of the range of p_r of practical interest.

For convenience write equation 4.2 as

$$i_i = AV_i^2 . \eta \ , \qquad \text{VIII.i}$$

where A is a constant.

The instantaneous power is

$$P_i = V_i i_i = AV_i^3 . \eta \ ,$$

and the energy absorbed over a quarter cycle is

$$W = A\int_{t_o}^{\pi/2\omega} \eta V_i^3 \, dt \ . \qquad \text{VIII.ii}$$

Division of W by the time $\pi/2\omega$ gives the mean power, which divided by the "optimum" power, AV_2^3, yields the result

$$\eta_{a.c} = \frac{2}{\pi}\left\{\left(1-\frac{V_o^2}{V_2^2}\right)^{1/2}\left(\frac{2}{3}-\frac{V_o^2}{6V_2^2}\right) - \frac{V_o}{V_2}\left(\frac{\pi}{4}-\frac{1}{2}\arcsin\frac{V_o}{V_2}\right)\right\} \qquad \text{VIII.iii}$$

This function increases as expected with V_2/V_o and is asymptotic to the value $4/3\pi$ ($\doteq 0.425$) as $V_2/V_o \to \infty$. It is shown plotted on fig.(4).

Case 2 $\eta_{d.c} = 1 - V_o^2/V_i^2$

Fig.(1) shows that this function gives an approximate lower bound of the family of curves of $\eta_{d.c.}$ versus V_2/V_o. A similar process to the last gives

$$\eta_{a.c} = \frac{4}{3\pi}\left(1 - \frac{V_o^2}{V_2^2}\right)^{3/2}, \qquad \text{VIII.iv}$$

which is also shown on fig.(4).

It may thus be expected from the above that the following exact calculation of $\eta_{a.c.}$ will give curves lying approximately between the above curves, for the practical range of p_r.

Complete analysis

As indicated earlier the problem is to integrate the product of instantaneous current and voltage over a quarter wavelength.

Thus $$W = \int_0^{\pi/2\omega} i_i V_i \, dt .$$

Now i_i and V_i are most conveniently expressed in terms of the dimensionless variable X (see equations 3.1, 3.2 and 3.3), so that dt must also be expressed in terms of X. The integral then becomes

$$W = \int_0^{X_2} i_i(X) V_i(X) \frac{dT}{dV_i}(X) \frac{dV_i}{dX}(X) \, dX ,$$

where X_2 is the value of X corresponding to the peak voltage V_2. The integrand is now evaluated term by term. From equation 4.1 in the main text it follows that

$$\frac{dT}{dV_i} = \frac{1}{\omega V_2 (1 - V_i^2/V_2^2)^{1/2}} . \qquad \text{VIII.vi}$$

From equations 3.1 and 3.2 the instantaneous voltage is

$$V_i = \frac{E_+^* \tau_o}{(1+X^2)^{1/2}} \left\{ (1+X^2 p_r^2)^{1/2} - (1+X^2)^{1/2} + \ln p_r + \ln \left[\frac{1+(1+X^2)^{1/2}}{1+(1+X^2 p_r^2)^{1/2}} \right] \right\} , \qquad \text{VIII.vii}$$

which when differentiated with respect to X becomes

$$\frac{dV_i}{dX} = \frac{E_+^* \tau_o X}{(1+X^2)^{1/2}} \left\{ \frac{p_r^2}{1+(1+X^2 p_r^2)^{1/2}} - \frac{1}{1+(1+X^2)^{1/2}} - \frac{X(p_r - 1)}{(1+X^2)\eta_{d.c}^{1/2}} \right\} . \qquad \text{VIII.viii}$$

From equations 3.2 and 3.3 the instantaneous current is

$$i_i = \psi . 2\pi\epsilon L k \qquad \text{(for a length L of duct)}$$

$$= \frac{2\pi\epsilon L k E_r^{*2} X^2}{(1+X^2)} . \qquad \text{VIII.ix}$$

Now if E_r^* is expressed by $E_r^* = V_o/r_o \, \ell n \, p_r$ (from equation 3.7), the terms given by equations vi, vii, viii and ix can be collected to give

$$i_i V_i \frac{dT}{dV_i}\frac{dV_i}{dX} = \frac{2\pi\epsilon k L V_o^4 X^4 R_1^2 (1-1/p_r)^2}{\eta_{dc}^{1/2}\omega V_2 p_r t_o (\ell n p_r)^4 (1+X^2)^2 \left(1 - \frac{X^2 V_o^4 p_r^2}{(1+X^2)\eta_{dc} V_2^2 (\ell n p_r)^2}\right)^{1/2}} \left\{A(X)\right\}, \qquad \text{VIII.x}$$

where

$$A(X) = \left\{ \frac{p_r^2}{1+(1+X^2 p_r^2)^{1/2}} - \frac{1}{1+(1+X^2)^{1/2}} - \frac{X(p_r-1)}{(1+X^2)\eta_{dc}^{1/2}} \right\},$$

and

$$\eta_{dc} = \frac{X^2 (p_r-1)^2}{\left\{(1+X^2 p_r^2)^{1/2} - (1+X^2)^{1/2} + \ell n p_r + \ell n \left[\frac{1+(1+X^2)^{1/2}}{1+(1+X^2 p_r^2)^{1/2}}\right]\right\}} .$$

Now from the definition of $\eta_{a.c.}$,

$$\eta_{a.c} = \frac{W . 2\omega (R_1 - r_o)^2}{\pi . 2\pi\epsilon L k V_2^3} ,$$

which gives

$$\eta_{a.c} = \frac{2}{\pi}\int_0^{X_2} \frac{X^4}{(1+X^2)^2}\left(\frac{V_o}{V_2}\right)^4 \frac{(p_r-1)^3}{\eta_{dc}^{1/2}(\ell n p_r)^4}\left(\frac{1}{1 - \frac{X^2}{(1+X^2)\eta_{dc}}\left(\frac{V_o}{V_2}\right)^2 \frac{p_r^2}{(\ell n p_r)^2}}\right)^{1/2}\left\{A(X)\right\} dX, \qquad \text{VIII.xi}$$

where $A(X)$ and $\eta_{d.c.}$ are as above, and

$$\left(\frac{V_o}{V_2}\right)^2 = \frac{(\ell n p_r)^2 (1+X_2^2)(\eta_{dc})_{X_2}}{p_r^2 X_2^2 (1-1/p_r)^2} \qquad \text{VIII.xii}$$

By the use of VIII.xi and xii, and by the choice of suitable values of X_2 and p_r, the parameters $\eta_{a.c.}$ and V_2/V_o may be calculated and plotted

against each other. Solutions obtained numerically for p_r = 20, 40 and 200 are shown on fig.(4) for comparison with the simplified solutions above. As expected the computed solutions fall between the two approximate curves shown, and again have the upper limit of $4/3\pi$. The Algol procedure used for the calculations is given in Appendix IX.

Appendix IX

Algol procedure for evaluation of $\eta_{a.c.}$ (see section 2.4.6)

Description of operation

Inspection of equation 4.3 shows that $\eta_{a.c.}$ is a function of X and p_r, as is $\eta_{d.c.}$. The procedure acEff provides this function by a numerical integration of equation 4.3; an analytical solution would be very difficult. An external procedure INTEGRATE is called, which uses Simpson's rule to integrate a given function between prescribed limits to a given accuracy. The main body of the procedure consists of assignment statements designed to provide the integrand with the minimum of computational time. Since the integrand becomes infinite at the upper limit the integration is truncated at a value of X/X_2 less than unity, and a correction term based on a simple expansion about $X = X_2$ is applied; it was, however, necessary to go to $X = 0.999999X_2$ to obtain sufficient accuracy.

The formal parameters p, q, r of acEff correspond to X, p_r and the required accuracy.

```
real procedure INTEGRATE (f,x,a,b,eps,h); value a,b,eps; real f,x,a,b,eps,h;
comment integrates f(x) between limits a and b with accuracy eps, starting
        interval h;
real procedure acEff (p,q,r); value p,q,r; real p,q,r;
comment p is the parameter X, q is the cylinder ratio p_r, r is accuracy required;
begin real procedure g(x); value x; real x;
    comment uses non local C2, qsqd, ℓnq. Supplies variable part of integrand;
    begin c,d,s,t,w,csqd;
        A: d := x x x; s := sqrt(1.0+dxqsqd); t := sqrt(1.0+d);
           c := (ℓn((1.0+t)/(1.0+s))+s-t+ℓnq)/t; csqd := c x c; w := C2-csqd;
           if abs(W)<10-8 then begin x := x-10-6; goto A end;
           g := (x/t)↑3.0/sqrt(W)x(cxqsqd/(1.0+s)-c/(1.0+t)-csqd/t)
    end g;
    real qsqd,m,ℓnq,v,u,C2,C1,X,vi,ui,xi,ci,xis;
    qsqs := q x q; m := p/20.0; ℓnq := ℓn(q); xi := p x 0.999999; xis := xi x xi;
    vi := sqrt(1.0+xis); ui := sqrt(1.0+qsqd x xis); v := sqrt(1.0 + p x p);
    u := sqrt(1.0 + qsqd x p x p); C1 := (ℓn((1.0+v)/(1.0+u))+u-v+ℓnq)/v;
    C2 := C1 x C1; ci := (ℓn((1.0+vi)/(1.0+ui)) + ui-vi + ℓnq)/vi;
    acEff := INTEGRATE(g(X),X,0.0001,xi,r x 1.57,m)x qsqd/C1↑3.0/
    1.5707963268 x (1.0-1.0/q)↑2.0 + ((xi/vi)↑2.0 + (p/v)↑2.0)x(ci+C1)
    x qsqd x (1.0-1.0/q)↑2.0 x sqrt(2.0x(1.0-ci/C1))
    /2.0 x 3.1415926536 x C1↑3.0;
end acEff;
```

Appendix X

Development of heater

Since several unexpected difficulties arose which delayed, and finally curtailed, the testing of the heater, it is pertinent to describe its development in some detail.

X i The insulators

The original design incorporated four glazed ceramic insulators, which were fitted in pairs at each end of the heater tube (see figs. 8 and 10). The spiders (fig. 11) locating the central (emitter) wire were mounted between each pair. The thickness of each insulator was 2.5 cm, which was thought to be sufficient to prevent surface tracking between the spider and earth on either side. This width was, during the high pressure tests, found to be inadequate, and an insulator at the upper end cracked owing to overheating caused by tracking. Replacements for the upper insulators were then made to similar dimensions of Sandanyo, with the central hole threaded to 3mm pitch to lengthen the tracking path (fig. 10). Since this material was hygroscopic the insulators were varnished in an attempt to seal them, but when tested they failed through the body at about 40 kV. The wire location at the upper end was then completely redesigned with much longer possible tracking paths, and made of Tufnol (fig. 12); at the same time the insulation thickness at the lower end was doubled (fig. 13).

X ii Emitter development

The main factor affecting the choice of emitter were its diameter, surface texture and material. Several experiments were conducted at atmospheric pressure in order to establish the best combination.

The work of Uhlmann[20] and Uhlig[4] had indicated the desirability of using a high cylinder ratio p_r in order to obtain a high breakdown field strength, by the formation of "steady burst pulse" corona (see section 3.3). However, the ratio necessary - about 400 - could not be achieved because the outer diameter was predetermined by heater design

requirements (section 2.5), and the wire had to be of sufficient diameter for mechanical strength and to withstand repeated sparking. In consequence the maximum ratio obtained was about 100, which meant that the corona was in the "streamer" phase (section 3.3). Two attempts were made to overcome this limitation:

1. The wire was replaced by a 10 B.A. brass screw thread in order to achieve the required very high field strength on the peaks. This method failed as streamers quickly formed on small imperfections on the thread, causing irregular current and premature spark breakdown.

2. The wire was heated in stages up to red heat (about 800°C), by passing through it an alternating current of up to 2A, RMS, and later (see below) a direct current of up to 1.5A. The cylinder was at high potential, the wire earthed. It was hoped by this means to create the "steady burst pulse" corona by the change in ion structure proposed by Uhlig[4], which was a change from molecular or colloidal to atomic form. Although this mode of corona was shown by Hermstein (see section 3.3) to have different causes, a progressive suppression of streamers did take place, both on visual and audible evidence. However, it was not possible to assess the effect on breakdown voltage, as oscillation of the wire which was present but not serious with the unheated wire reached an amplitude of half the gap at $1\frac{1}{2}$A, resulting in early breakdown. The wire heating experiments were stopped at this stage, largely because of the difficulty of arranging, within the pressure vessel, a power supply to the wire, which was at high potential.

Attention was then directed to the problem of wire oscillation, which it was thought might be aggravated by the greater forces involved in the pressure vessel. The oscillation was only slightly reduced by the change from a.c. to d.c. wire heating, and was not affected by variation of the wire tension or diameter. It was finally reduced to a small amplitude by the insertion of a P.T.F.E. spider upstream of the centre of the tube, to act as a spacer (see fig. 11).

The materials used for the tests were Kanthal and nickel, there being no noticeable difference in performance between them. Platinum was used for some later tests, and showed a much greater resistance to fusing on sparking, owing to its higher melting point.

Appendix XI

Determination of starting field strength and ion mobility from experimental results (radial field system)

Since the theory for the current-voltage relationship requires a knowledge of the quantities E_r^* and k, it is useful to be able to determine these experimentally instead of having to rely on published or assumed values.

The relationship may be written (see equations 3.3 and 3.5):

$$\eta^{-1} = \frac{V_2^2}{\psi (R_1 - r_0)^2}$$

But η is a function of the variable X, with the cylinder ratio p_r as a parameter (see equation 3.6), so that for a given p_r, η^{-1} may be given as a function of X. But since $E_r^{*2}/\psi = 1 + 1/X$ (from equation 3.2) it is preferable to plot η^{-1} versus $1 + 1/X$. The curve thus represents

$$\frac{V_2^2}{\psi (R_1 - r_0)^2} \quad \text{versus} \quad \frac{E_r^{*2}}{\psi}$$

Some curves for various values of p_r are shown in fig. 16.
Now the experimental variables measured are V_2 and i/L, p_r and ϵ being known. Thus recalling the definition of ψ (equation 3.3) it is possible to plot $\frac{V_2^2 \cdot 2\pi\epsilon k_1 L}{i (R_1 - r_0)^2}$ versus $\frac{2\pi\epsilon k_1 L E_{r_1}^{*2}}{i}$ from experimental results, where k_1 and $E_{r_1}^*$ are "dummy" assumed values. If both theoretical and experimental curves are drawn on a logarithmic basis to eliminate effects of scale, the fit then gives the ratios between k_1 and k, and between $k_1 E_{r_1}^{*2}$ and $k E_r^{*2}$, from which the desired true values k and E_r^* are determined directly. The latter can of course be checked approximately by noting the voltage V_0 at which a very small current (say 10 μA) was observed and calculating E_r^* from the formula $V_0 = E_r^* r_0 \ell n p_r$.

Appendix XII

Radial field pressure rise (see section 6.1.4)

Consider a cylindrical duct with electrodes of radii R_1 and r_o. Let the charge density be expressed by

$$\rho(r) = \frac{\rho_g \alpha Q_o}{e} ,$$

where ρ_g is the gas density and e is the electron charge. Then the radial pressure gradient may be written

$$\frac{dp}{dr} = e\rho(r).E(r). \qquad \text{XII.i}$$

Now from Poisson's equation, (See Appendix III),

$$\rho(r) = \frac{\epsilon}{er}\frac{d}{dr}(rE_r) . \qquad \text{XII.ii}$$

Also, from equations III.iv and III.v,

$$\frac{d}{dr}(rE_r) = \frac{\psi}{E_r} \qquad \text{XII.iii}$$

Substitution of equations XII.ii and XII.iii into XII.i now gives, on integration:

$$\Delta p = p_{R_1} - p_{r_o} = \epsilon \int_{r_o}^{R_1} \frac{\psi}{r} dr ,$$

giving $$\Delta p = \epsilon \psi \ln p_r , \qquad \text{XII.iv}$$

or, from equation 3.5 in the main text,

$$\Delta p = \frac{\epsilon V_2^2}{(R_1 - r_o)^2} . \eta \ln p_r , \qquad \text{XII.v}$$

where $\eta < 1$.

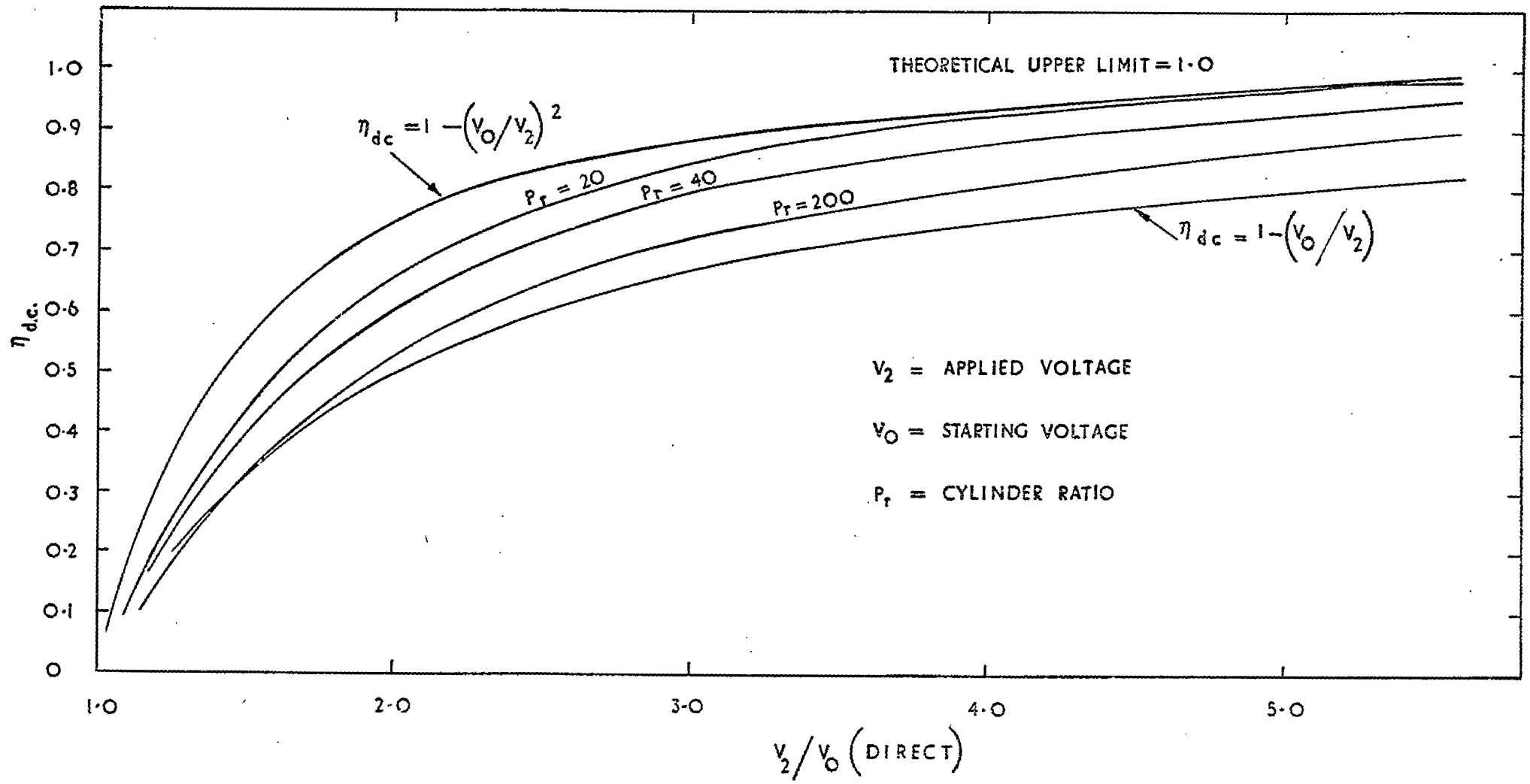

FIG 1 VARIATION OF $\eta_{d.c.}$ WITH APPLIED VOLTAGE

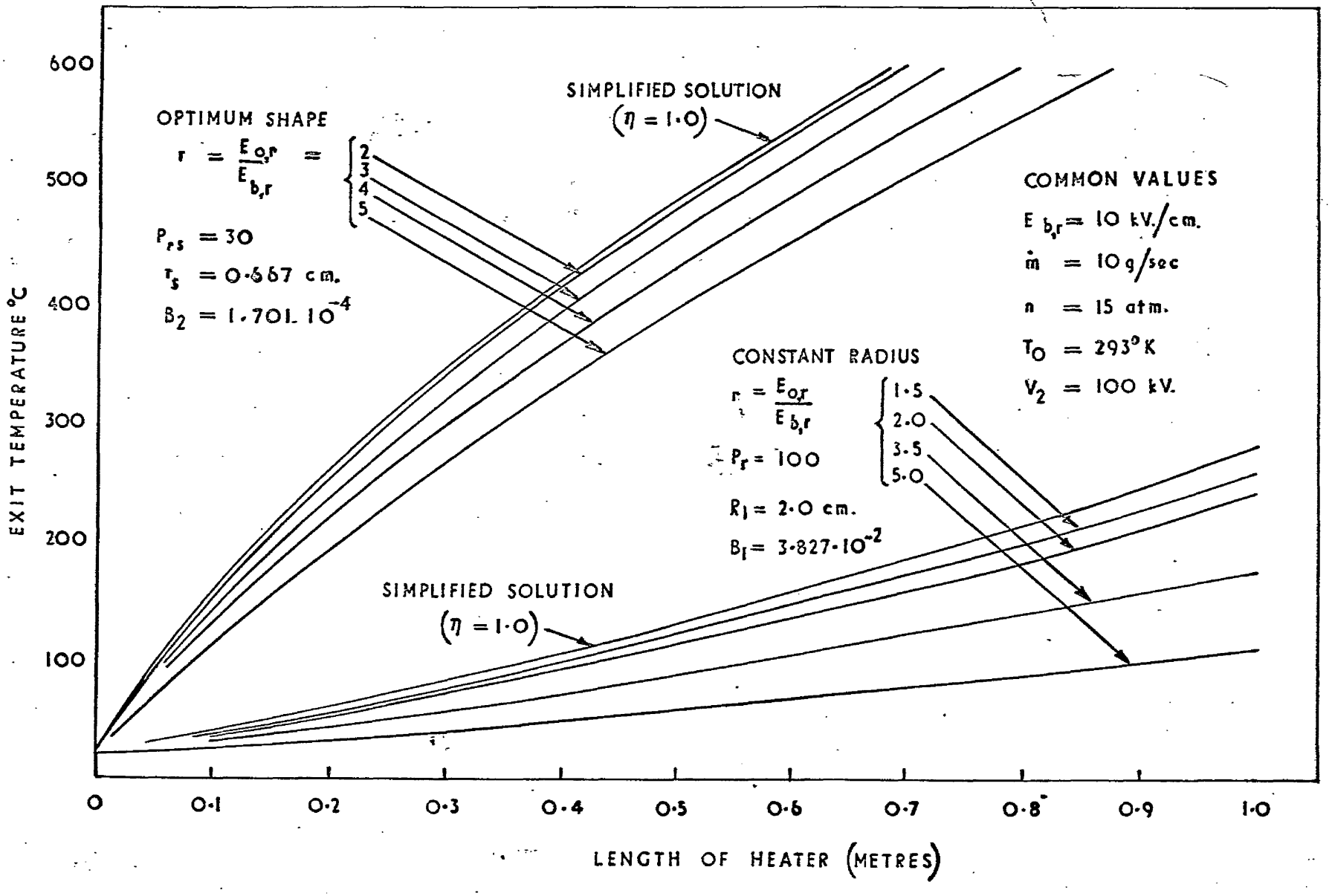

FIG 2 VARIATION OF EXIT TEMPERATURE WITH LENGTH OF HEATER

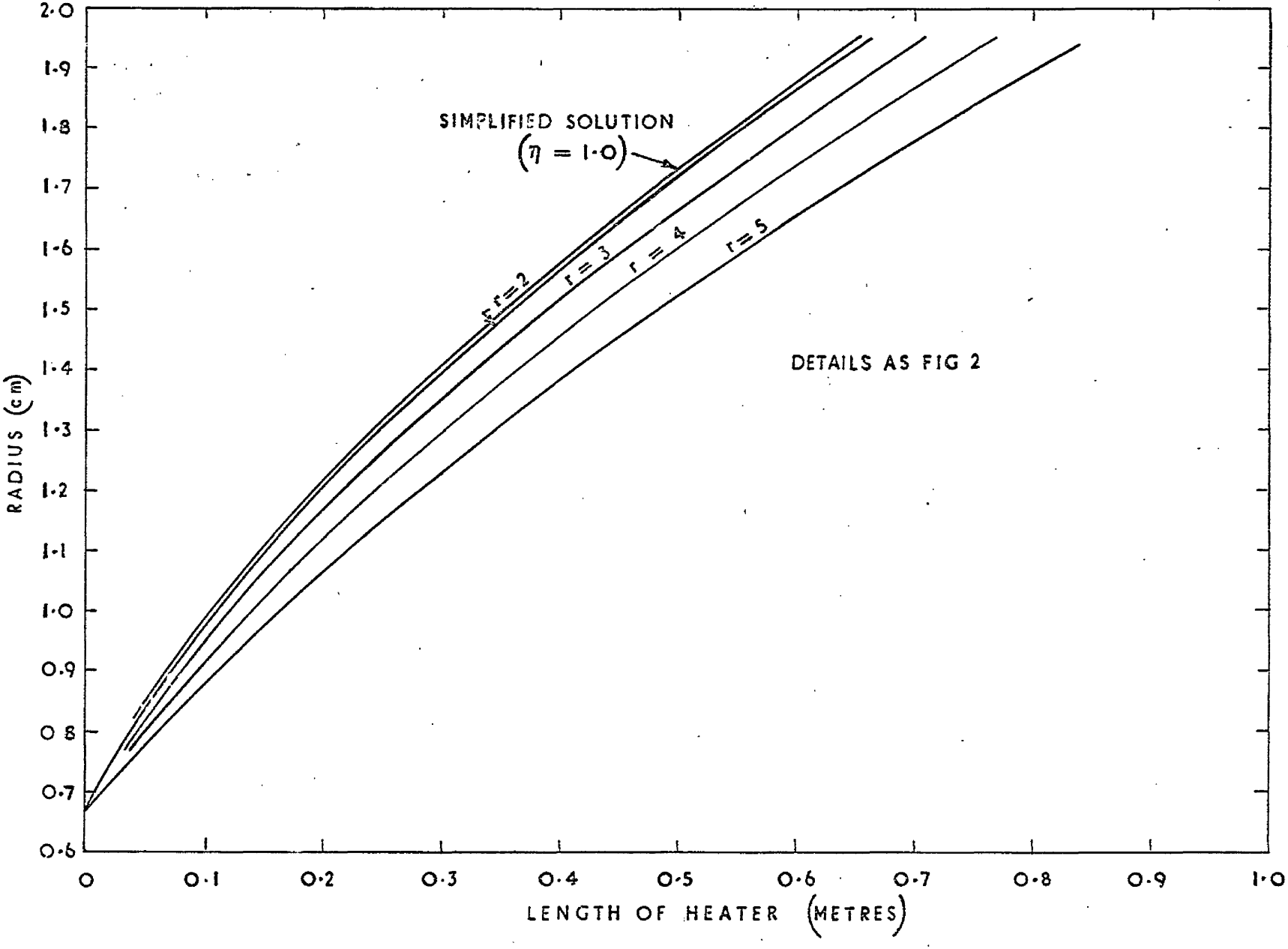

FIG 3 SHAPE OF OPTIMUM HEATER

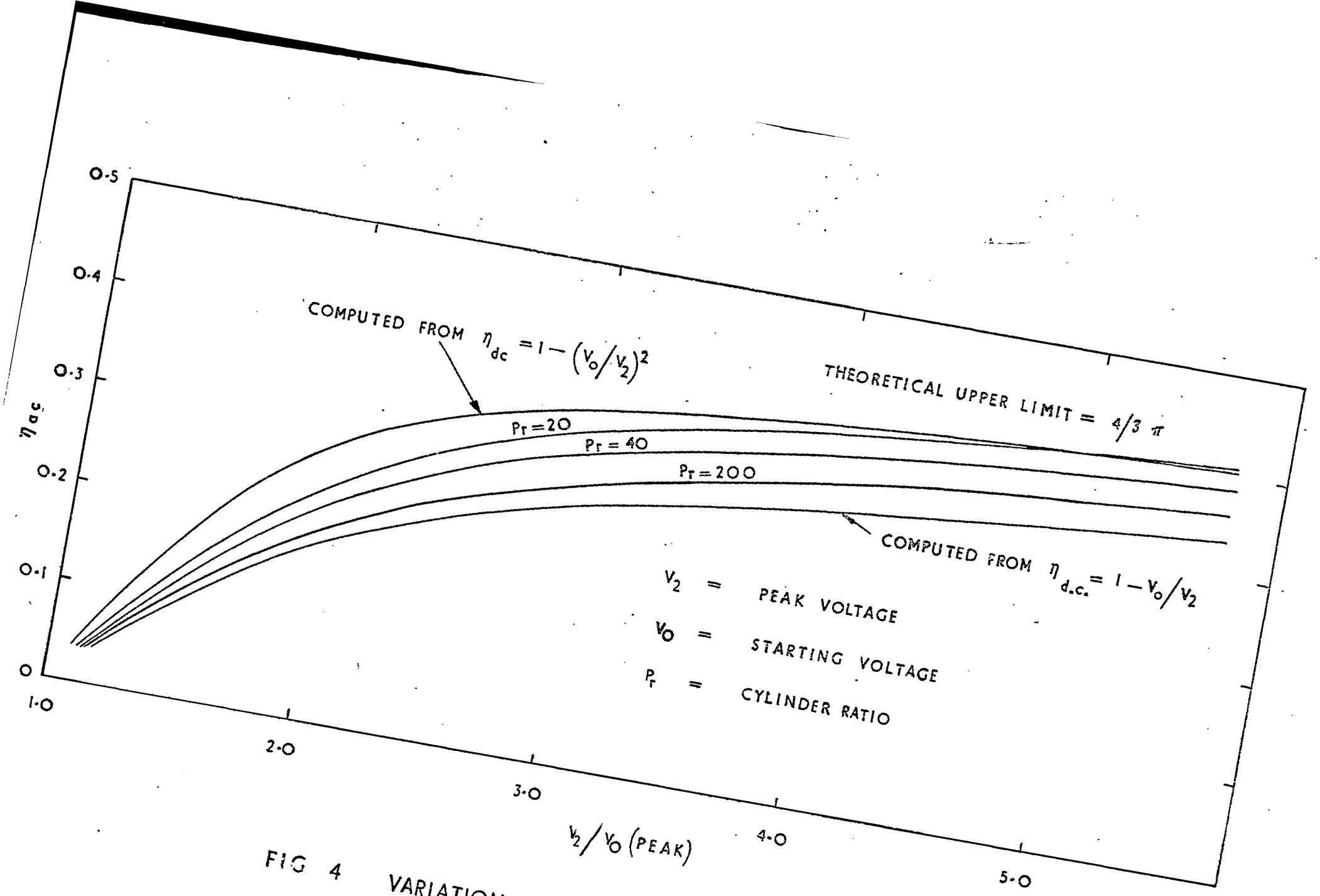

FIG 4 VARIATION OF η_{ac} WITH APPLIED VOLTAGE

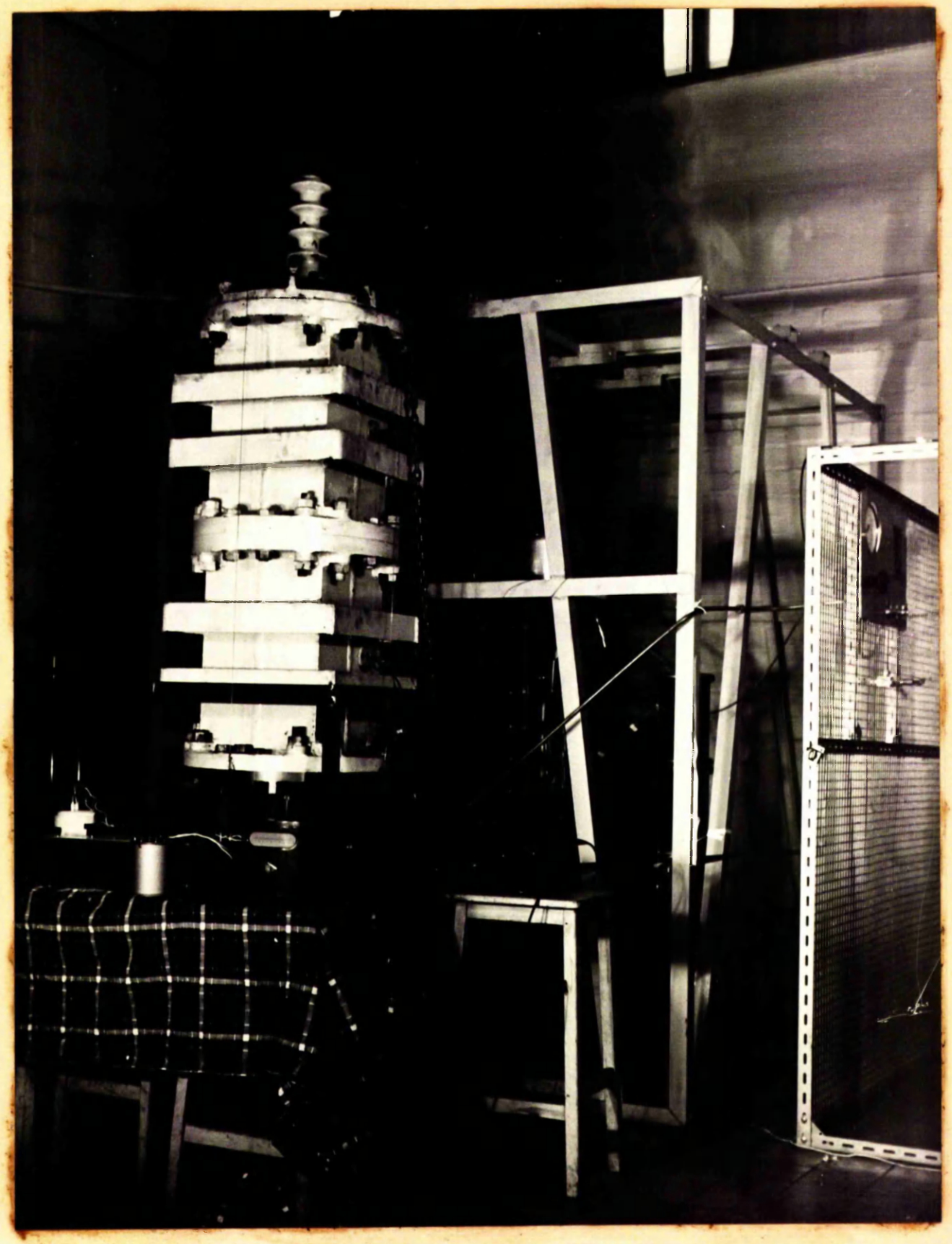

FIG 5 GENERAL VIEW OF APPARATUS (1)

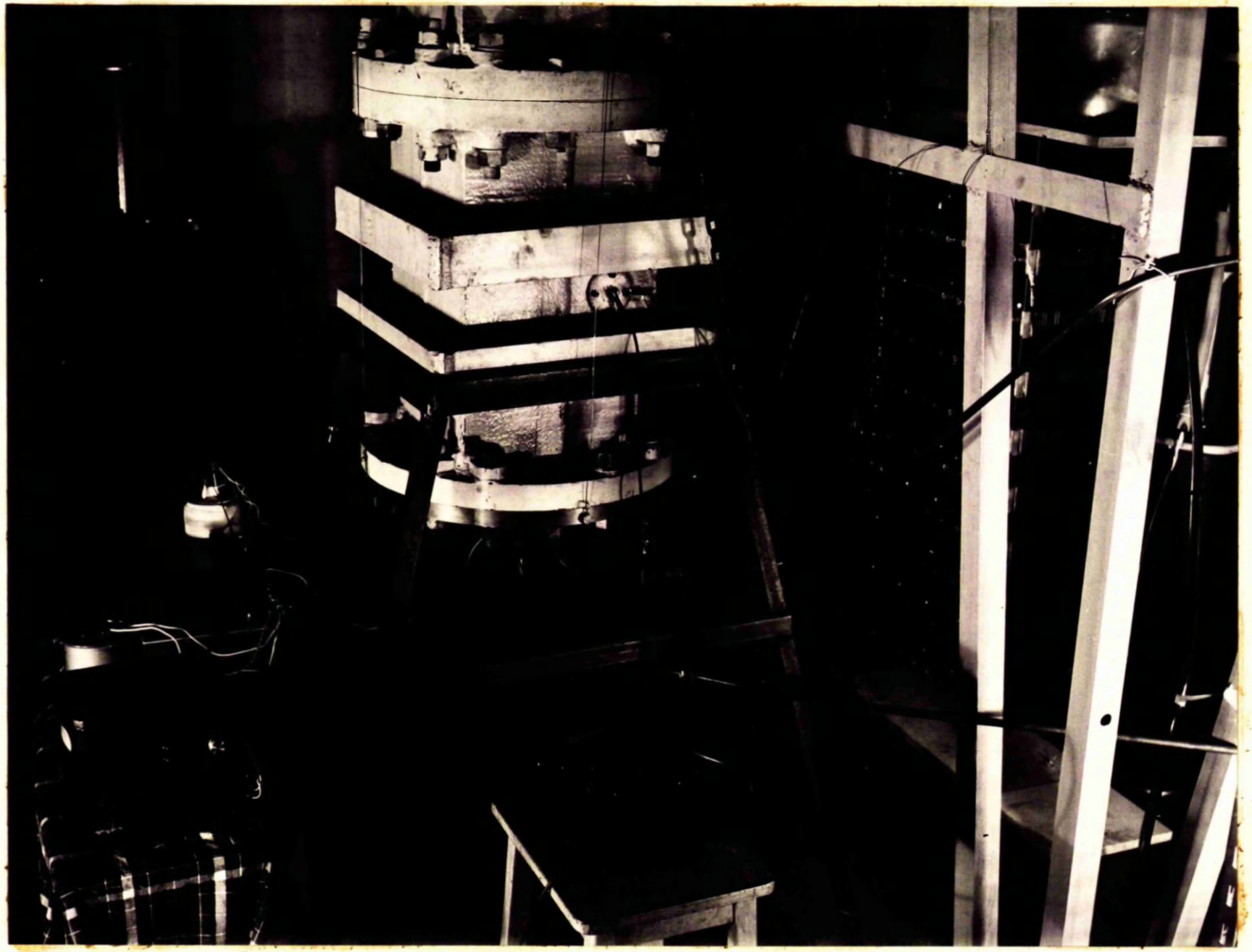

FIG 6 GENERAL VIEW OF APPARATUS (2)

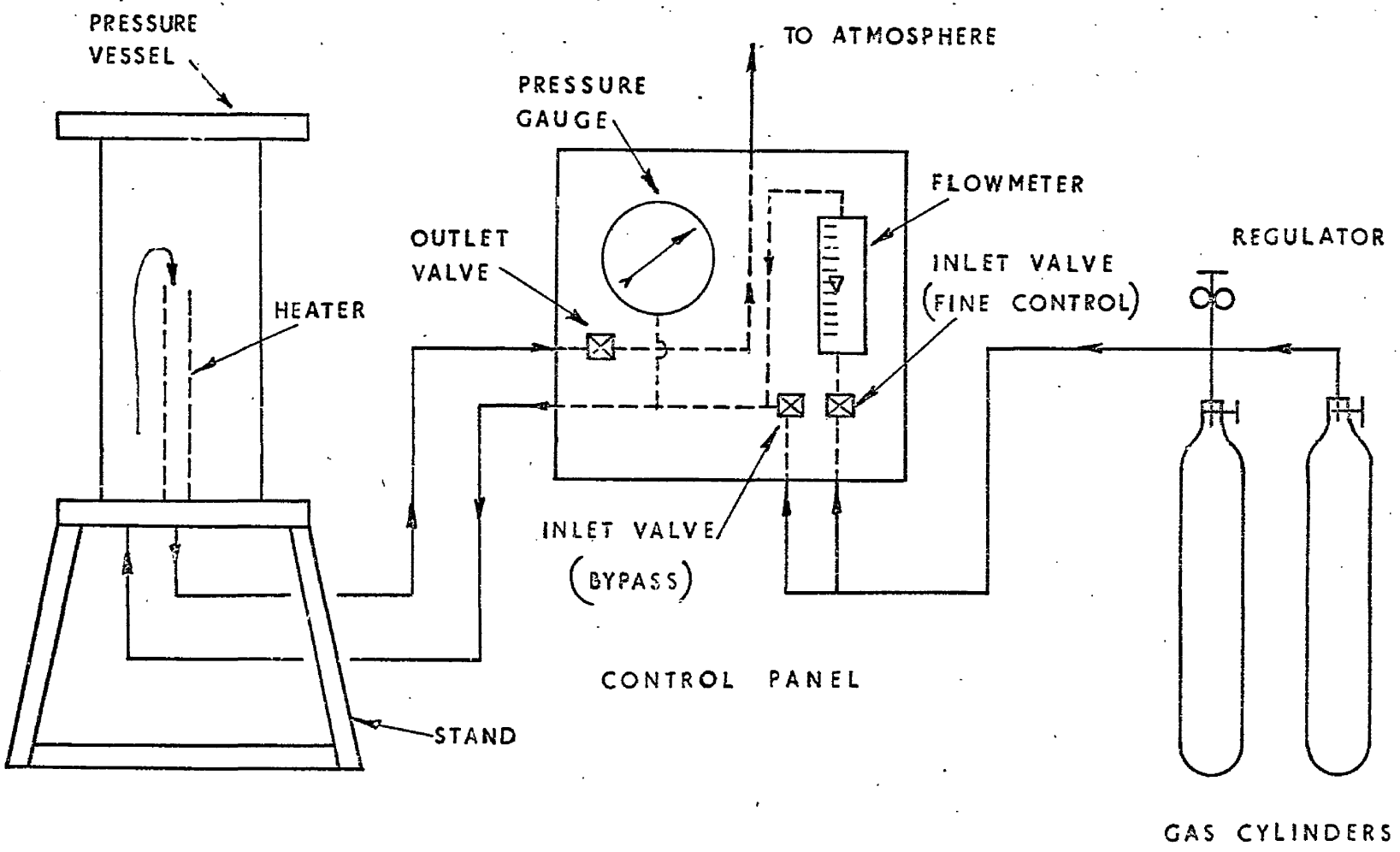

FIG 7 SCHEMATIC DIAGRAM OF GAS SUPPLY SYSTEM

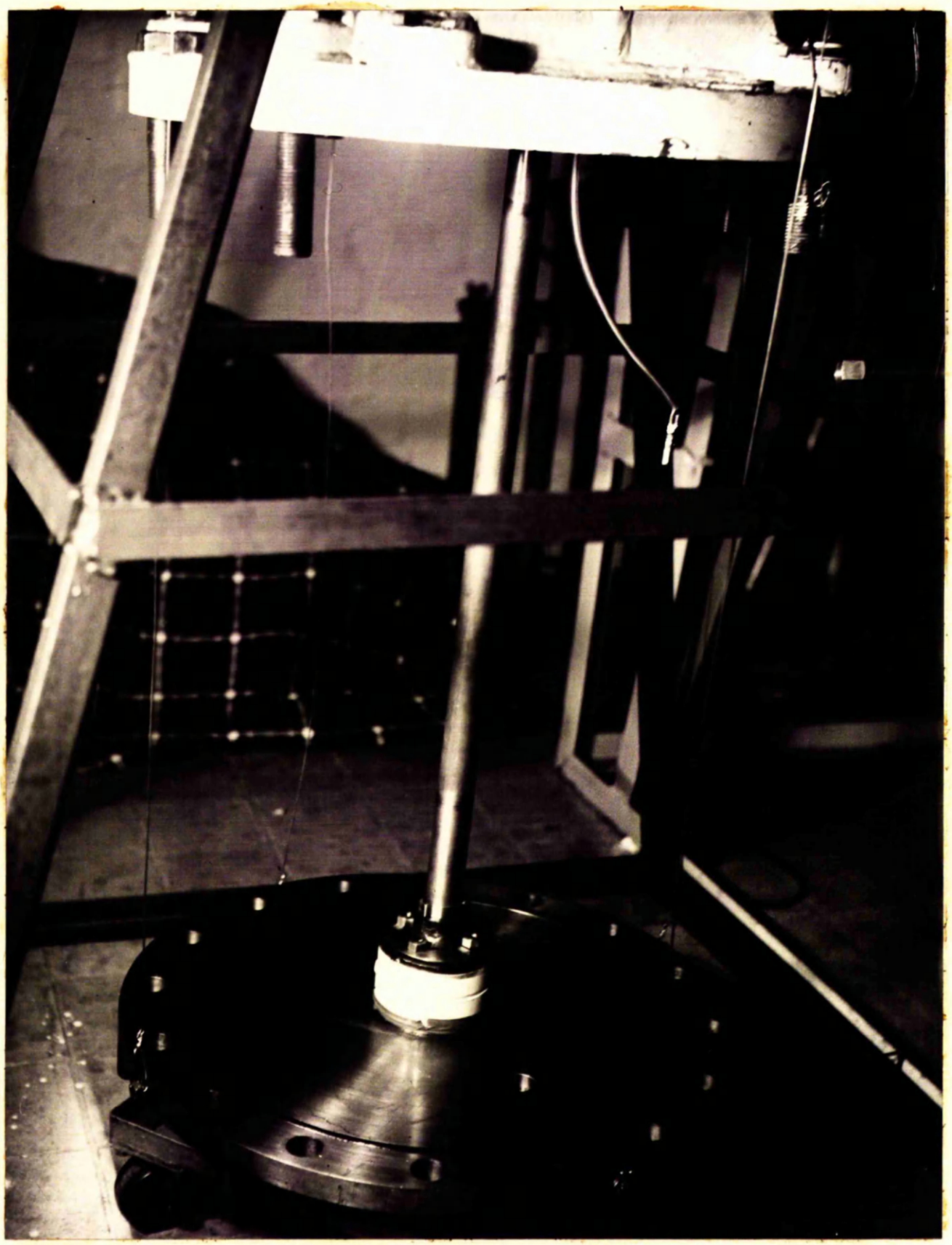

FIG 8 HEATER ATTACHMENT AND BOTTOM PLATE

FIG 9 BOTTOM PLATE SHOWING GAS AND THERMOCOUPLE CONNECTIONS

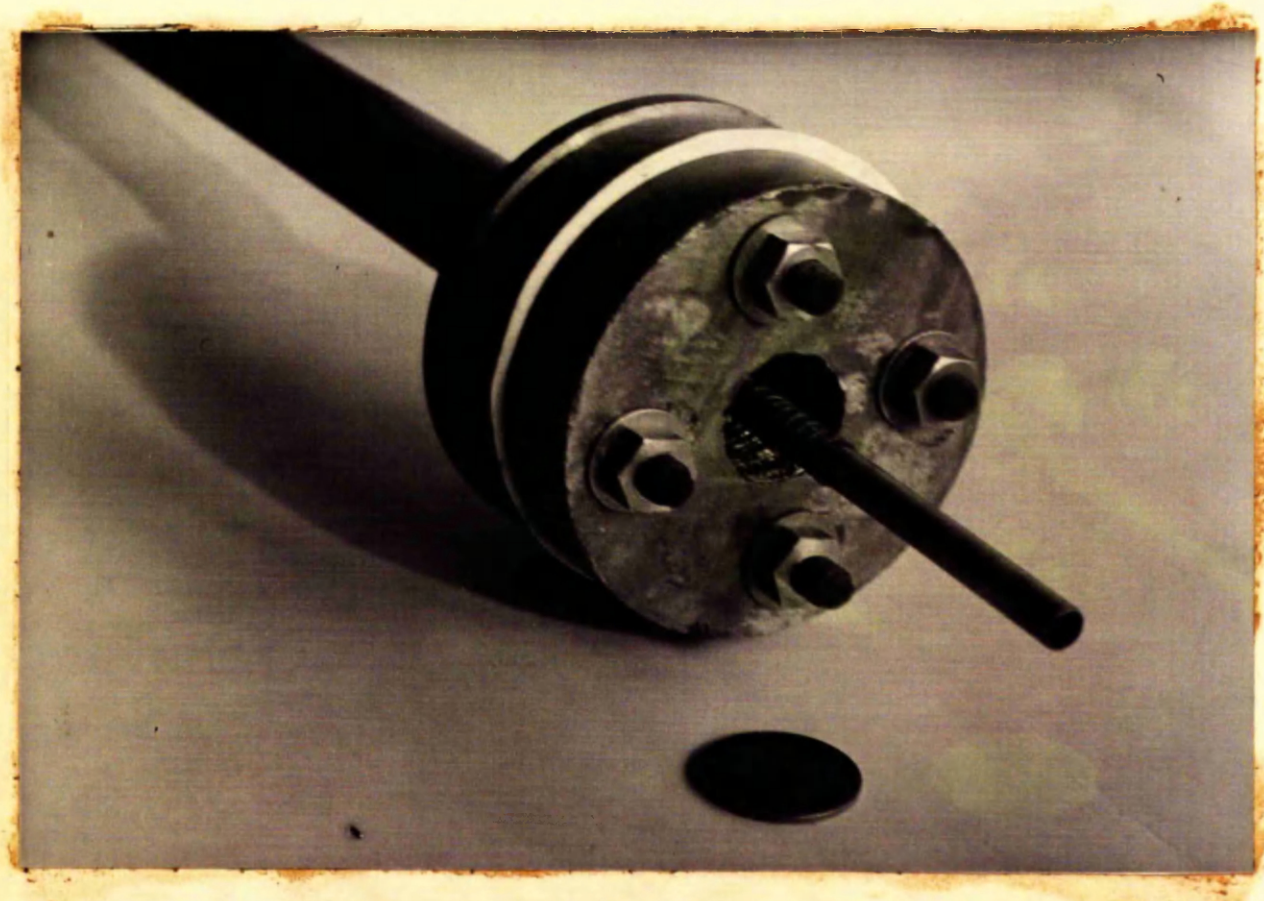

FIG 10 ORIGINAL UPPER INSULATORS SHOWING SPRUNG CONNECTOR

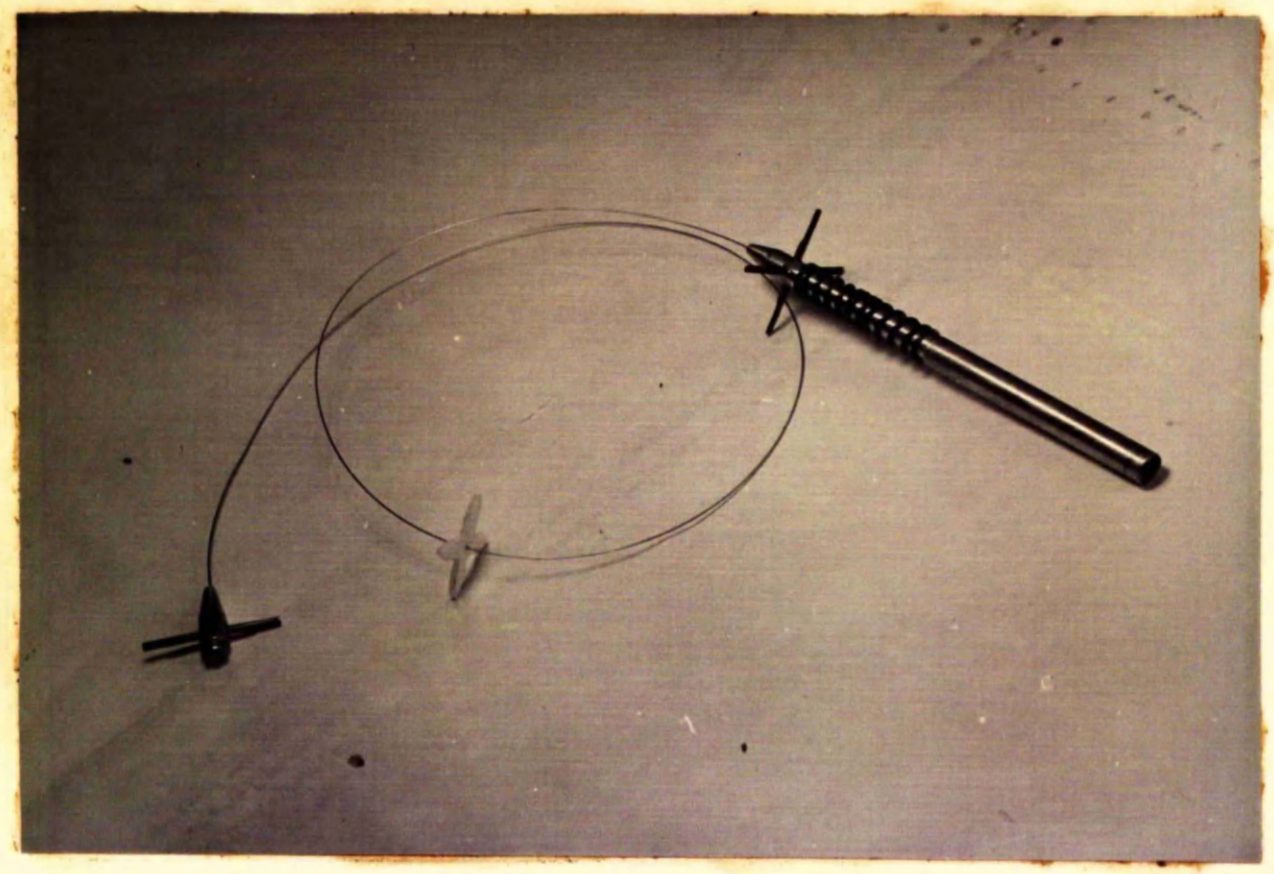

FIG 11 WIRE EMITTER SHOWING SPIDERS

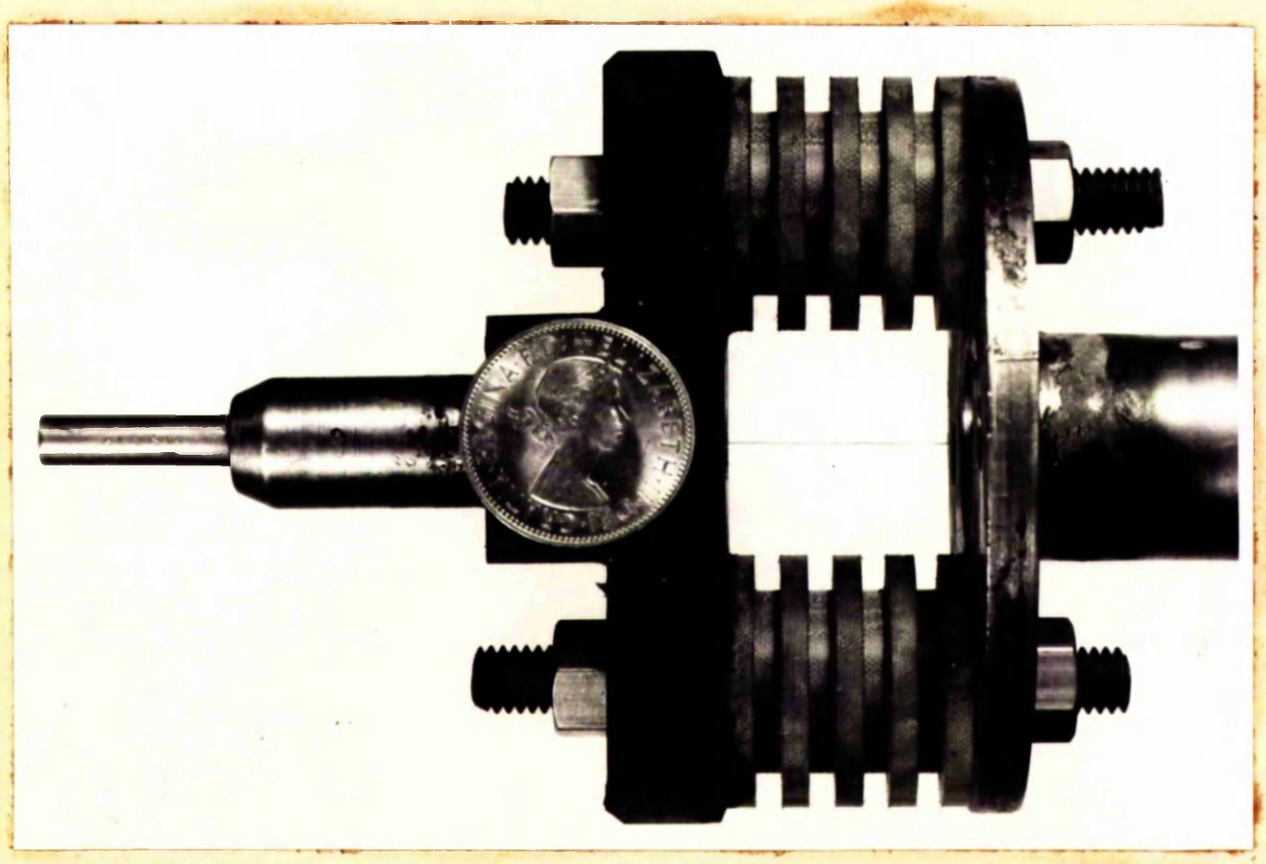

FIG 12 FINAL UPPER INSULATORS

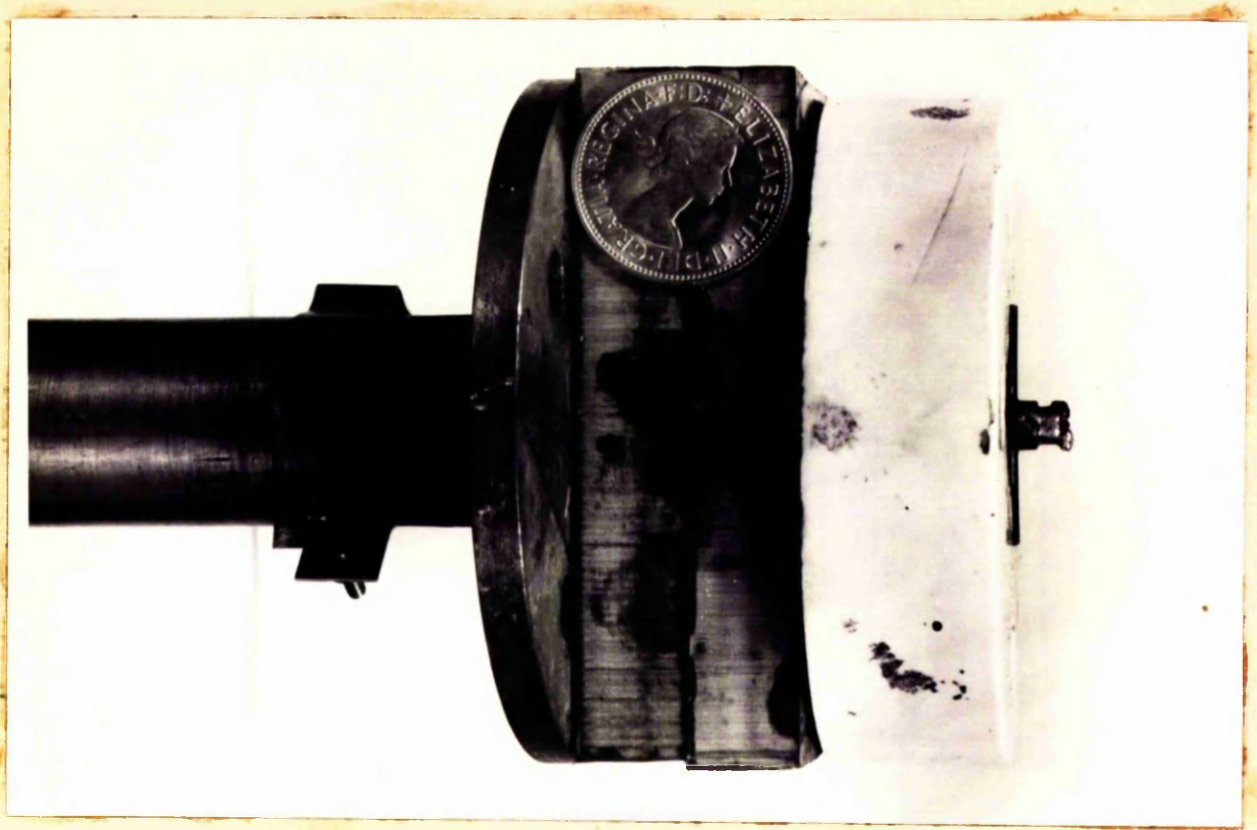

FIG 13 FINAL LOWER INSULATORS

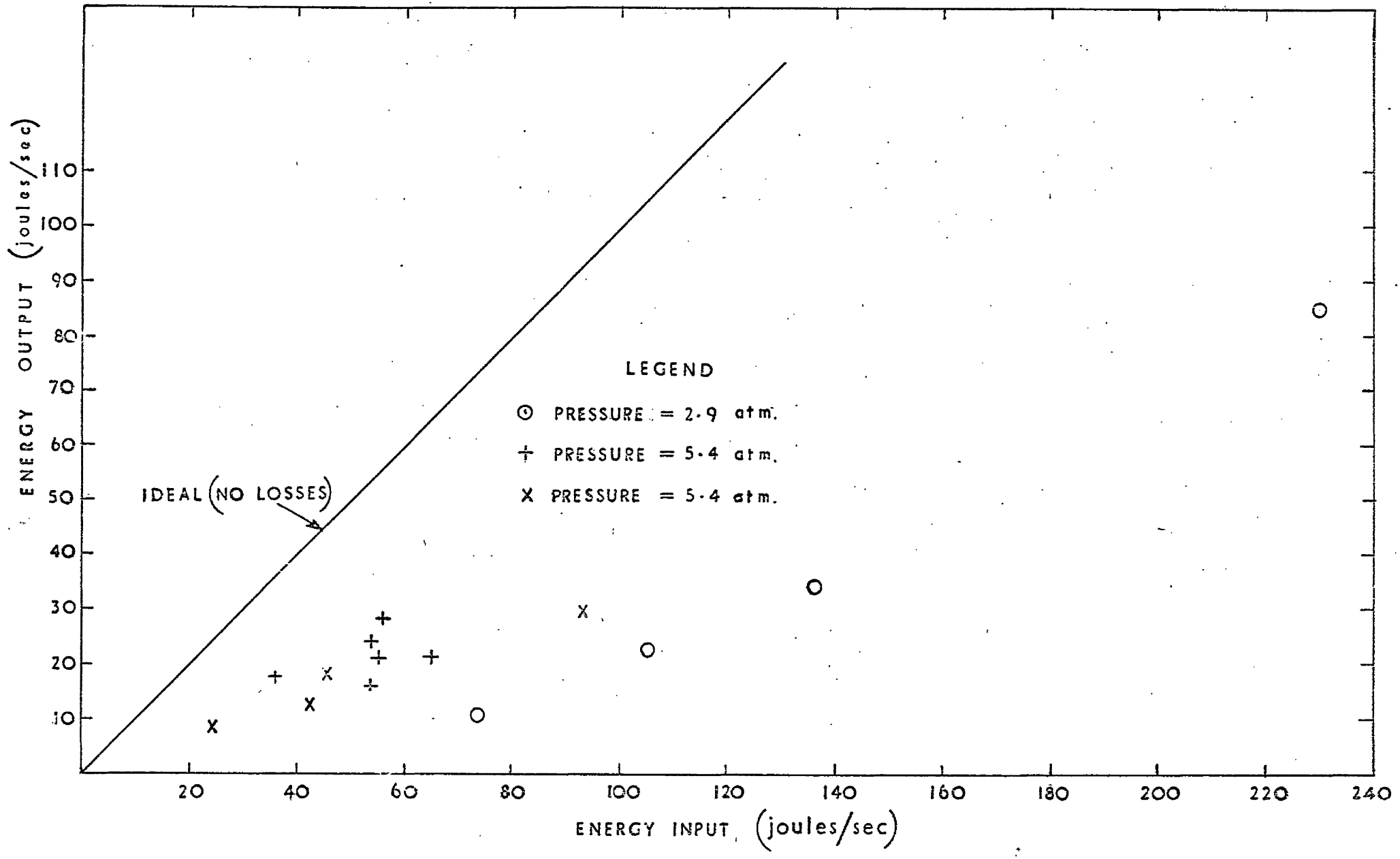

FIG 14 HEATER RESULTS

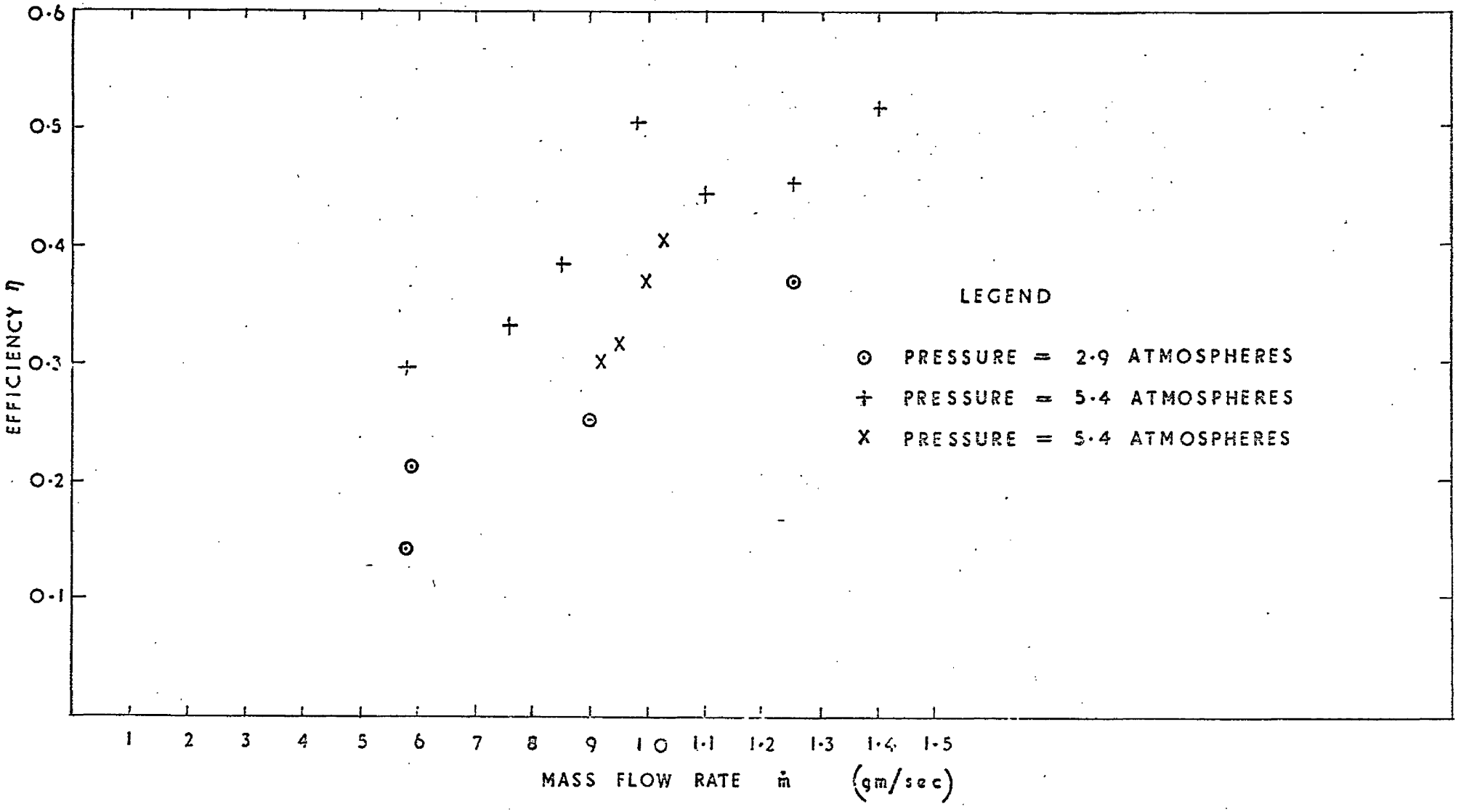

FIG 15 VARIATION OF EFFICIENCY OF ENERGY TRANSFER WITH MASS FLOW RATE

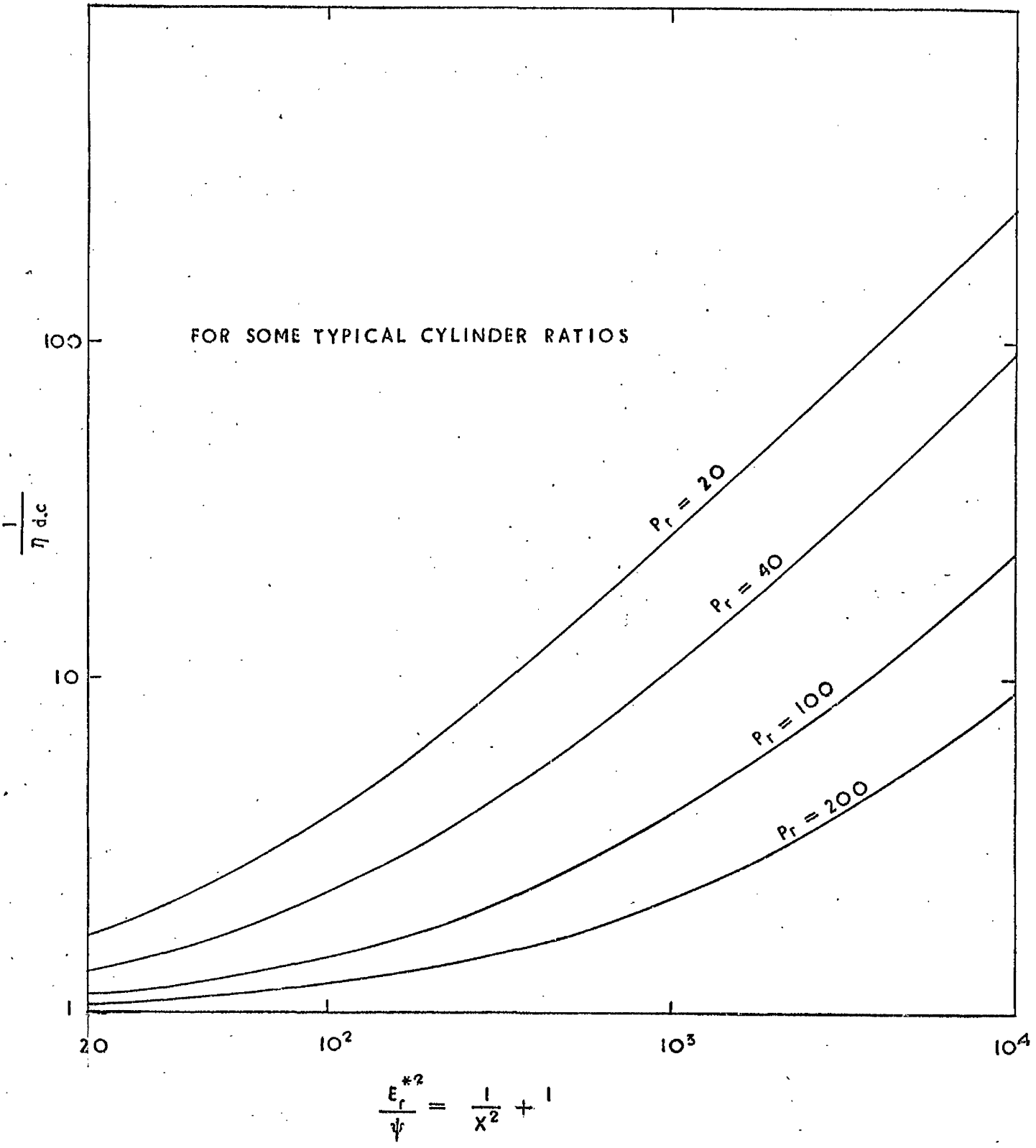

FIG 16 THEORETICAL-CURRENT VOLTAGE RELATIONSHIP

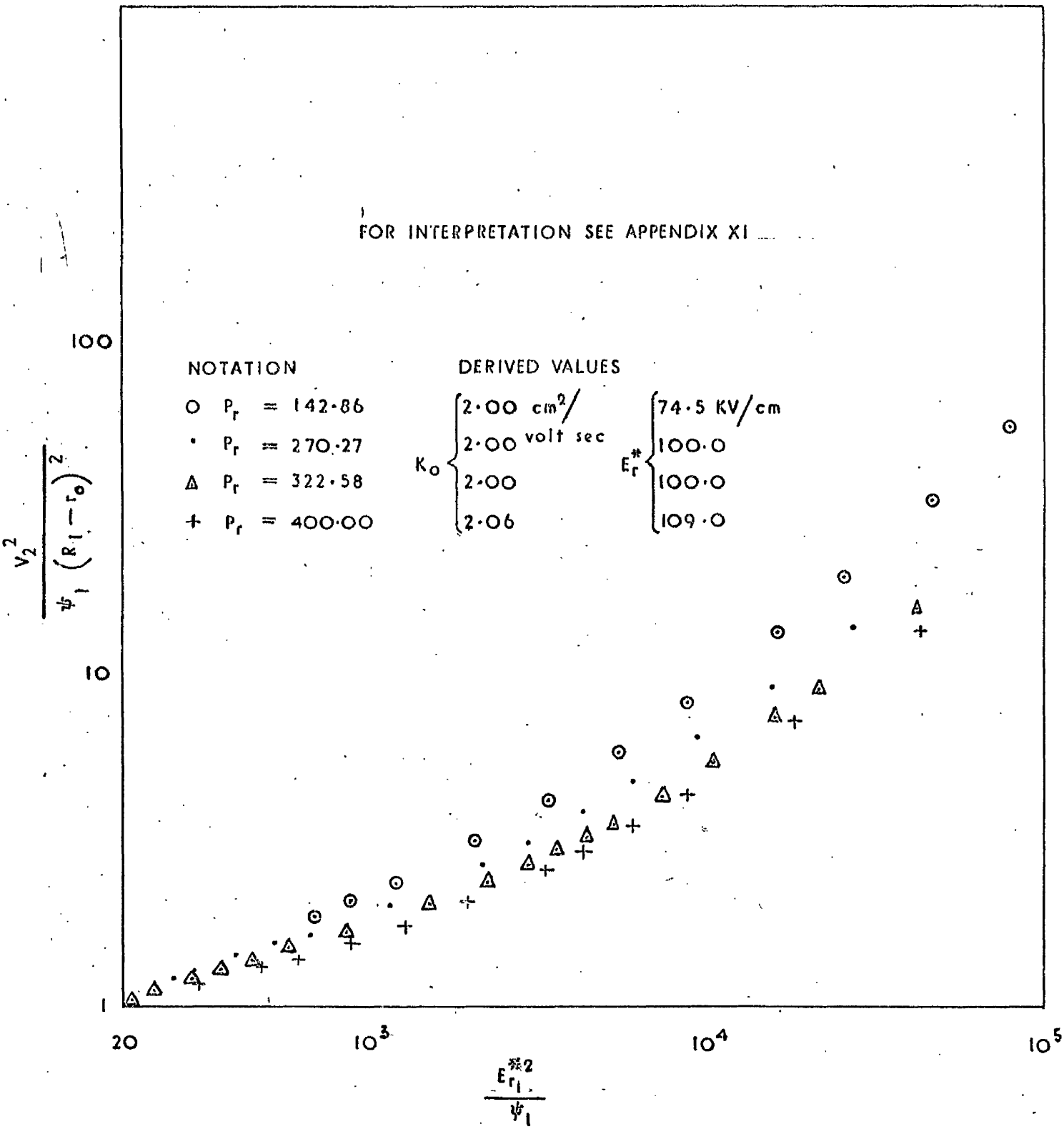

FIG 17 EXPERIMENTAL CURRENT VOLTAGE RELATIONSHIP

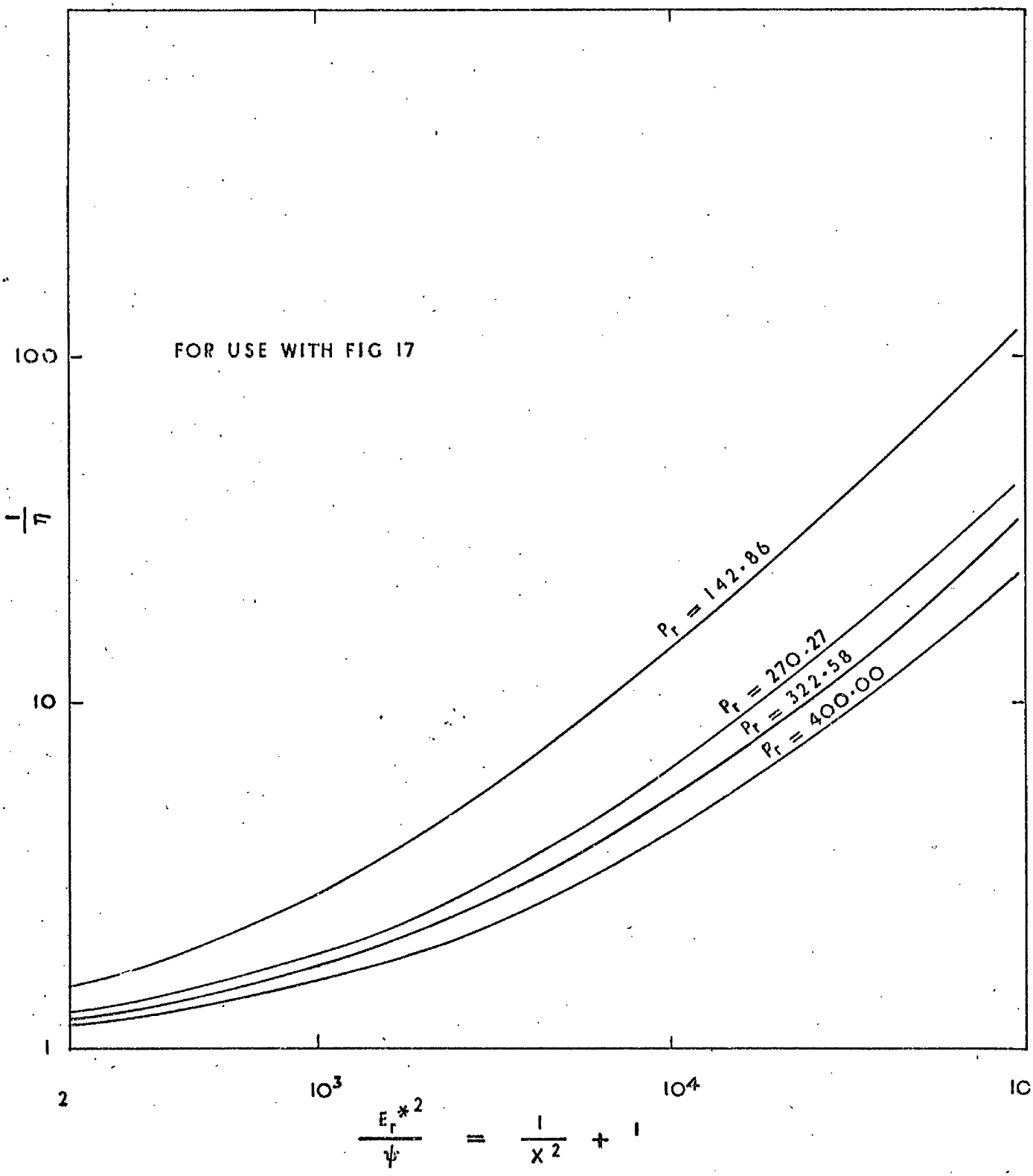

FIG 18 THEORETICAL CURRENT–VOLTAGE RELATIONSHIP

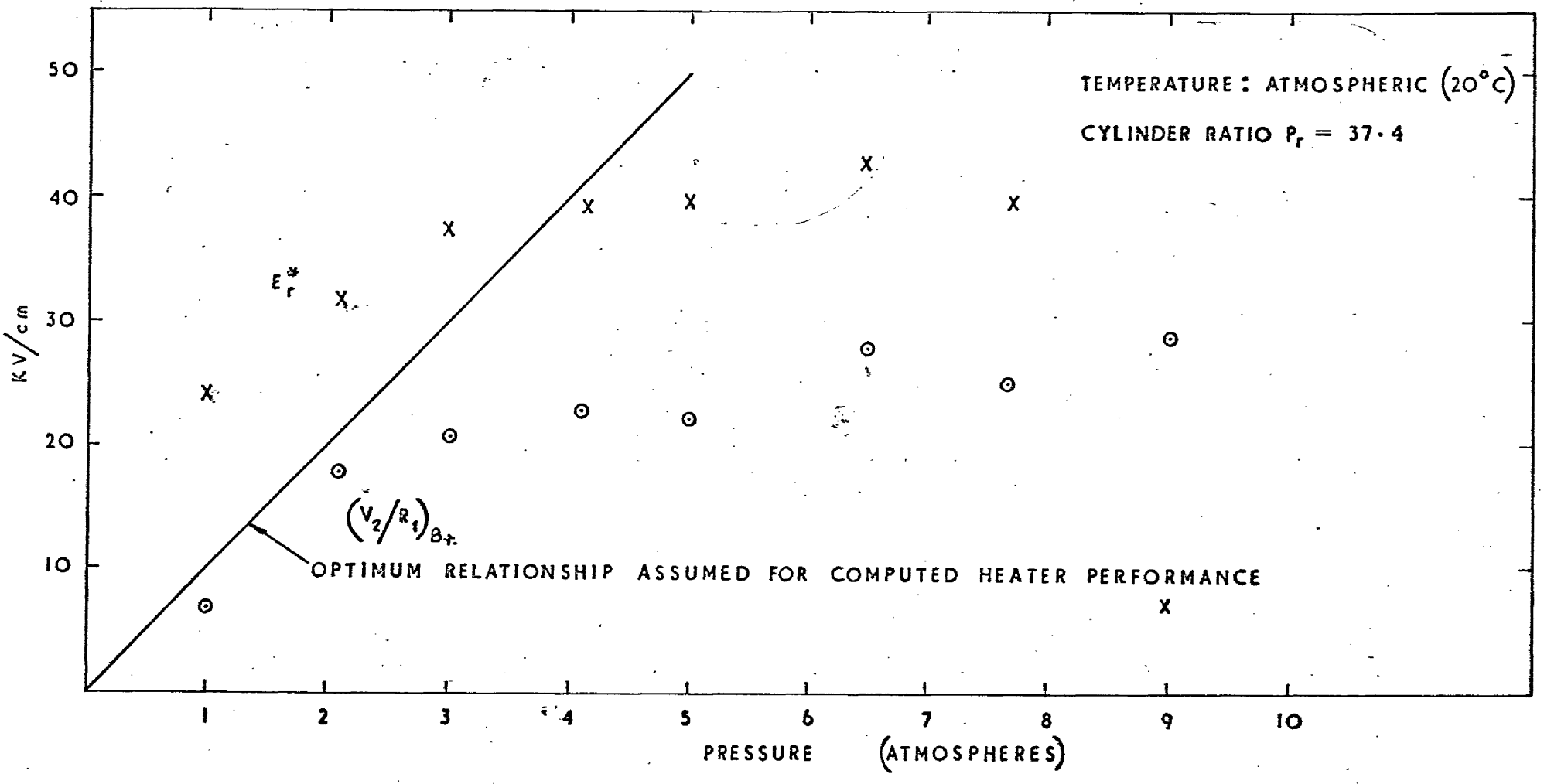

FIG 19 VARIATION OF STARTING AND BREAKDOWN FIELDS WITH PRESSURE

TABLE 1 Results of heating experiments

i mA	V kV	iV watt	T_ℓ °C	ΔT °C	$\dot{m}$ gm/sec	$\dot{m}C_p\Delta T$ joule/sec	η conversion efficiency
•	Run 1 : Pressure = 2.9 atm.						
3.20	23.0	73.6	37.0	18.0	0.58	10.45	0.142
6.50	21.0	136.4	57.0	38.0	0.90	34.20	0.251
11.50	20.0	230.0	87.0	68.0	1.25	85.00	0.370
6.10	17.3	105.0	58.0	39.0	0.58	22.60	0.215
+	Run 2 : Pressure = 5.4 atm.						
12.00	20.0	240.0	106.0	87.0	1.25	108.90	0.453
3.60	18.0	64.9	47.0	28.0	0.76	21.20	0.332
2.00	18.0	36.0	37.5	18.5	0.98	18.10	0.504
3.20	17.4	55.7	39.5	20.5	1.40	28.70	0.515
3.10	17.5	54.2	40.8	21.8	1.10	24.00	0.442
3.20	17.3	55.4	44.0	25.0	0.85	21.20	0.384
3.10	17.3	53.6	46.5	27.5	0.58	15.90	0.298
x	Run 3 : Pressure = 5.4 atm.						
1.63	26.0	42.4	33.0	14.0	0.92	12.90	0.304
4.80	19.5	93.6	50.2	31.2	0.95	29.60	0.317
2.72	16.8	45.7	37.0	18.0	1.03	18.50	0.406
1.81	13.5	24.4	28.0	9.0	1.00	9.00	0.369